JPRS-CST-86-039

23 SEPTEMBER 1986

China Report

SCIENCE AND TECHNOLOGY

FBIS FOREIGN BROADCAST INFORMATION SERVICE

NOTE

JPRS publications contain information primarily from foreign newspapers, periodicals and books, but also from news agency transmissions and broadcasts. Materials from foreign-language sources are translated; those from English-language sources are transcribed or reprinted, with the original phrasing and other characteristics retained.

Headlines, editorial reports, and material enclosed in brackets [] are supplied by JPRS. Processing indicators such as [Text] or [Excerpt] in the first line of each item, or following the last line of a brief, indicate how the original information was processed. Where no processing indicator is given, the information was summarized or extracted.

Unfamiliar names rendered phonetically or transliterated are enclosed in parentheses. Words or names preceded by a question mark and enclosed in parentheses were not clear in the original but have been supplied as appropriate in context. Other unattributed parenthetical notes within the body of an item originate with the source. Times within items are as given by source.

The contents of this publication in no way represent the policies, views or attitudes of the U.S. Government.

PROCUREMENT OF PUBLICATIONS

JPRS publications may be ordered from the National Technical Information Service, Springfield, Virginia 22161. In ordering, it is recommended that the JPRS number, title, date and author, if applicable, of publication be cited.

Current JPRS publications are announced in Government Reports Announcements issued semi-monthly by the National Technical Information Service, and are listed in the Monthly Catalog of U.S. Government Publications issued by the Superintendent of Documents, U.S. Government Printing Office, Washington, D.C. 20402.

Correspondence pertaining to matters other than procurement may be addressed to Joint Publications Research Service, 1000 North Glebe Road, Arlington, Virginia 22201.

JPRS-CST-86-039

23 SEPTEMBER 1986

CHINA REPORT

SCIENCE AND TECHNOLOGY

CONTENTS

ABSTRACTS

/12223

NATIONAL DEVELOPMENTS

SINO-JAPANESE TECHNOLOGICAL COOPERATION DETAILED

Beijing CHINA DAILY SUPPLEMENT in English 31 Jul 86 p 5

[Text] The Chinese and Japanese governments progressed in depth and breadth in 1985 in terms of scientific and technological cooperation.

In 1985 the two governments brought their strength into full play and reinforced their cooperative research on an increasing number of mutually rewarding scientific and technological projects. The number of cooperative items agreed on at the third session of the Sino-Japanese Scientific and Technological Cooperation Mixed Committee held last April in Beijing outstripped the combined total of the previous years.

According to the agreements concluded at the session, the Chinese and Japanese scientists have conducted joint research on nearly 30 subjects in about a dozen fields together. The two succeeded in extracting niobium (Nb) from molten iron, and are now applying for a patent on the process and are preparing for the industrial test. This new technique is expected not only to facilitate the comprehensive utilization of China's complex minerals, but also to be profitable as well.

Cooperation

Scientists from China and Japan also scored a significant progress in their research into antibiotics for both agricultural and medical use. From a soil sample provided by the Chinese, the team discovered a new set of antibiotics. The experiments and studies showed that one of these new kind of insecticide that will be more effective, safe and less toxic than others used for grey mycosis of cucumber, anthracnose, tomato and rice blights. Another three may be effective against leukaemia and other cancers and tumours. The patent rights for these new antibiotics are being applied for jointly by the two sides.

Technical cooperation here means the transfer of Japanese technologies to China. In 1985 Japanese companies with the help of their government provided China with equipment and a set of grants worth 45 million yuan (US$14 million).

In 1985, the Chinese Government sent more than 200 scientists, technicians, economists and managerial personnel to Japan for training. China also invited more than 100 Japanese specialists from various fields to lecture or give technical guidance to their counterparts in China. At present, the two sides are cooperating in the construction of research bases and personnel training centers in China. The centers will focus on the areas of meat, fish and timber production, irrigation and water conservation projects, climatic control, medicine, family planning, business management and the management of post and telecommunications. When opened, these centers will contribute to the development of Chinese research in these fields, while improving the capabilities of Chinese personnel.

Chinese and Japanese experts have made feasibility surveys of some of China's key construction projects, which include harbours, railways, water conservation projects, mining, expressways, subways and environmental protection projects. Chinese and Japanese scientists have also studied the possibilities of technically upgrading some of China's small and medium-sized enterprises. In addition, the Japanese have provided some Chinese institutions with scientific research and medical equipment. The two governments also agreed to promote cooperative activities between their youths. Starting in 1986, young Japanese technicians will travel to China to help with its scientific, technological and educational development.

Mutual Visits

As the above indicates, cooperation between the two sides has now expanded into various fields and is of vital significance to the scientific and economic development of both countries.

Apart from cooperative agreements, 1985 also saw frequent mutual visits between government leaders, scientists and technicians.

In the spring of 1985, a Chinese delegation headed by State Councillor Fang Yi attended the China Day activities of the Tsukuba International Science and Technology Exhibition, which opened on March 17. At the same time, the Chinese Government also sent out 800 additional representatives to the exhibition. While there, the group made contact with Japanese people from all walks of life.

The ministers of the two governments in charge of science and technology participated together in the Fourth Sino-Japanese Government Members Conference in Tokyo held July 30-31 and during which the two signed a cooperation agreement on the peaceful use of nuclear energy. The agreement opened a new area for scientific and technological cooperation between the two countries and showed that cooperation has become integral to Sino-Japanese friendly relations.

Exchanges

Takeuchi Reichi, Japan's former state minister for science and technology visited China at the invitation of Song Jian, minister in charge of the State Science and Technology Commission. Reichi's visit to China was the first for a Japanese minister in charge of scientific and technological work. The two sides had beneficial talks on scientific and technological cooperation and exchangees and decided to strengthen their ties in a variety of areas including exchanges between the decision-making departments of science and technology.

The recent developments demonstrate that great potential exists for Sino-Japanese scientific and technological cooperation. In 1986 it is hoped that the two countries will make the most of their advantages and expand the number of their cooperation projects. Only such cooperation can measure up to the developing friendly relations between China and Japan and fulfil the wish of the people of both countries, particularly those working in scientific and technological fields.

/9317
CSO: 4010/2019

PRC STUDENTS IN U.S. 'PLAN TO COME HOME'

Beijing CHINA DAILY in English 15 Aug 86 p 3

[Article by Wu Jingshu]

[Text]

Most Chinese students studying abroad intend to come back to work in China after their graduation, an on-the-spot survey has indicated.

Tang Ying, a Taiwan-educated scholar living in New Jersy, who interviewed 90 mainland Chinese students in the US last month, told China Daily that she was deeply impressed by the students' obvious affection for their homeland.

They all knew that there may be better opportunities for them if they stayed and worked abroad after graduation, but most of them did not hesitate to state their decision to return home "because they were Chinese," she said.

"The important point is that we should trust these young people and believe they can make the right decision in the ultimate interest of their country and themselves," she pointed out.

More than 90 per cent of Chinese students who have gone to study abroad over the past eight years have returned to work in China after graduation, according to a leading official of the State Education Commission.

During the six years from 1978 to 1985, China sent 36,000 students to study in 76 foreign countries on government subsidies. So far, more than 16,000 who finished their studies have returned home to work on assigned posts across China, while the others are continuing their studies abroad. Li Chengping, department director of the State Education Commission, said.

About 8,000 Chinese student went to study abroad during this period at their own expense. Most of them are still studying, while some of them have returned or taken up jobs abroad after graduation, Li added.

"It is our firm decision to continue sending Chinese students to study abroad during the country's Seventh Five-Year Plan period (1986-90), both on government expenses and through individual arrangements," Li said. "However, we will put more emphasis on short-term (one to two years) study tours for scholars and specialists to produce quick results in the country's development programme.

"The government, meanwhile, has decided to take all possible steps to improve work and study conditions for the returned scholars so that they can make good use of their knowledge once they take up assignments at home," Li said. Equal opportunities will also be provided for returned graduates who had studied abroad at their own expense, he added.

According to Tang Ying, most Chinese students she interviewed, while stating their intention to return home after graduation, told her that they were concerned whether the places where they would be working after returning home could provide proper conditions for them to carry on the research and development they had started abroad.

/9317
CSO: 4010/2019

MARKET, STRATEGY FOR DEVELOPING CIVIL AIRCRAFT

Beijing GUOJI HANGKONG [INTERNATIONAL AVIATION] in Chinese No 6, Jun 86 pp 2-4

[Article by Cheng Feng [3089 7364]]

[Text] Current Status and Main Problem Areas

Since the establishment of the People's Republic, China's aviation industry has grown from practically nothing to an industrial system with established production capability and a complete industrial base. The development of the civil aircraft has followed a rocky path for the past 30 years, during which time China has developed medium and small turboprop aircraft such as the Y-5, the Y-7, and the Y-11, as well as longer-range large aircraft such as the Y-8 and the Y-10. During the past few decades, the Y-5 has become an important aircraft in special aviation applications and on intra-provincial routes; it has made unquestionable contributions to China's aviation industry. The Y-7 aircraft is now in mass production, and a limited number have been used on a trial basis for air transportation in this country. The development of the Y-10 was an attempt to test our own production capability in building a large turbogan civil aircraft; it has given us considerable amount of experience and insight. These achievements not only provided valuable experience and an industrial base for further development of China's civil aircraft industry, but more importantly, they produced a highly trained technical team with expertise in developing civil aircraft.

However, we must admit that China's civil aviation industry had a rather late start, and its course of development has been quite turbulent; in fact, even today we still have not been able to find an effective course to develop the civil aircraft industry that is considered appropriate for this country. The main problems today are: out-dated aircraft design, lack of mature technologies, and poor reliability; as a result, the economic and technical performance indices of China's aircraft lag far behind those of other countries. In the area of aircraft production, no organization or structure has been established to promote civil aircraft development; neither has an operational system been established to promote cooperation and cross-fertiliation between military and civil aviation.

Prospects for the Immediate Future

A number of comprehensive studies have been conducted to address the problem of China's civil aircraft development; special articles have also been published on the topics of technical feasibility and market demand. However, there has been no in-depth studies on the prospects of China's civil aircraft development in the immediate future. A good understanding of this problem will have a direct impact on the policy to develp the market and strategy for China's civil aviation; in fact, it will directly affect the success or failure of the civil aircraft industry. To address this problem, I believe we should start by assessing the technical capability of China's aviation industry and the market demand, and utilize both foreign and domestic resources in conducting analyses and research.

First, let us review the civil aircraft market in this country. Up to now, the civil aircraft produced in China has been unable to establish a firm footing in the air transportation market. On the other hand, China's air transportation has been growing rapidly since 1973 primarily because of its poor initial condition. Under the state's new relaxed internal policy and open-door foreign policy, China's economy is enjoying an unprecedented boom, which has propelled the development of the air transportation industry. But due to the shortage of equipment, the demand cannot be met even though there has been an increase in the number of aircraft this year. The growth of China's air transportation provides favorable conditions for the development of the civil aircraft industry. It should be pointed out that based on the construction and age of China's current aircraft fleet, a significant portion of them wil be retiring from service after 1990. Considering this fact and the projected increase in demand for domestic air transportation, the present time is a critical period which provides a perfect opportunity for developing our civil aircraft industry.

Recognizing this scenario, many foreign aircraft manufacturers are engaged in a fierce battle to compete for the Chinese market. The market strategies of these foreign companies are not only aimed at current sales, but also designed to fill the void in the 1990's in anticipation of the aging aircraft being retired from service; they are trying to gain control of the present market opportunity so they can enjoy market monopoly for more than 10 years. Generally speaking, the average renewal cycle of an air transportation fleet is 15-25 years. If we lose this opportunity, we will not have another one until the next peak aircraft retirement period.

The above analysis shows that China's civil aircraft development is facing a critical period. If China's aviation industry fails to produce a technically and economically mature and advanced aircraft in time to meet the needs of the air transportation industry, then our civil aircraft market will be filled by foreign aircraft because to maintain China's economic growth, we cannot allow our air transportation to become stagnant or depressed. If this scenario ever comes to pass, our own civil aircraft industry may suffer a severe blow, and may become depressed for a long time to come. The joint military-civil aviation industrial system will become a pipe dream, and the advancement and stabilization of China's aviation

industry will be adversely affected. Therefore, the importance of developing China's civil aircraft before the year 2000 must be fully appreciated because it not only relates to the development of the civil aircraft itself but also affects the rate of growth of the entire aviation industry.

The Impact and Role of Market and Strategy Research in Civil Aircraft Development

I believe the impact and role of market and strategy research in civil aircraft development can be summarized in the following two areas:

Assessing the Demand for Civil Aircraft and Evaluating the Feasibility and Size of the Market

The basic elements propelling the development of civil aircraft are the growth rate of the national and regional air transportation industry and the number and type of aicraft needed. Without forecasts and analyses of the future development of air transportation, without comprehensive analyses and research of the air route structure, fleet formation and operating cost, it would be impossible to obtain an objective and accurate estimate of the future growth in air transportation and the number of aircraft needed; as a result, development of the civil aircraft industry will proceed in complete darkness, and this will inevitably lead to errors. As an example, let us consider the number of aircraft needed for domestic airlines. First, we must determine China's economic growth and the total air transportation needs for the next few years. Second, we must determine the types of aircraft that will be used for the domestic air routes. Third, we must assess the current status of the existing aircraft fleet and their future retirement period. Finally, we will be in a position to determine the number and types of aircraft needed, which represents the feasibility and size of the civil aircraft market. This market research should make use of information relating to the global economy, the regional economy, and the economy of the transportation industry; it should utilize knowledge in aircraft technology and economics to estimate the future prospects of China's air transportation industry and the formation and size of the aircraft fleet. This research should include continuous monitoring and analysis of the new situation and the development trend of China's air transportation industry. Only through continuous and independent research of market feasibility can we establish confidence in the estimated aircraft needs; we should not generate our estimates based only on some temporary conditions.

Determining the Direction of Production and Aircraft Models for Future Development

Based on the forecast of growth in air transportation, we can determine the direction of production for civil aircraft. Specifically, we should first evaluate our aircraft production capability and then determine the direction of production and the basic aircraft models for future development based on the aircraft type which has the highest market demand. If we make a wrong decision about the direction of production and aircraft models, the entire project will be doomed to failure even if the aircraft is a technological

success. Because the success or failure of aircraft development depends not only on its technical and economical performance but also on the market demand; in other words, the demand for the aircraft must exceed the required number that corresponds to the profit-low break-even point of the basic production line. A technically successful aircraft which has a demand of only a few dozen units will inevitably result in very high unit cost and poor sales. Therefore, aircraft market research is one of the most important sources of information for establishing policies to determine the direction of production, the basic models and ultimately the success or failure of the project.

Basic Methods of Market and Strategy Research

The market and strategy research of civil aircraft development plays an important role in the aircraft manufacturing industry. A number of today's major aircraft manufacturers in the world have established systematic and complete market research organizations, and have developed their own methods of research. Although the market research systems and methods differ from one another, the basic principles and procedures are essentially the same; they generally contain the following three major elements.

Forecast of Air Transportation Growth and Planning of Aircraft Fleet

The forecast of growth in air transportation involves using the method of econometrics to study the effect of national or regional economic development and other social factors on air transportation. The method of econometrics uses the theory and method of mathematics, economics, and statistics to establish mathematical models for a particular region or for the entire nation which define the relationship between air transportation and economic development and other factors. These models are then used to predict the number of passenger kilometers (RPK) at a specified time in the future.

The planning of an aircraft fleet involves determining the composition and size of the fleet based on the air route structure and existing fleet composition. The basic method uses information such as the aircraft production rate, daily utilization rate, flight frequency and fleet retirement plans, etc., to arrive at the number of aircraft required to meet the projected future passenger kilometers.

Detailed Development Issues and the Design of Technical and Economic Performance Indices

The results of market research also provide the basic data for aircraft design. For example, design parameters such as aircraft layout, structure, take-off weight, take-off distance, engine thrust, cruising altitude, speed, range, fuel consumption and direct operating cost must be estimated on the basis of market demand. In addition, the effect of using new technology in aircraft design must also be considered in determining the preliminary aircraft configuration.

Analysis of Potential Market Share of Civil Aircraft

As pointed out earlier, the success of an aircraft project depends not only on its technical and economic performance, but more importantly on its market share, i.e., the number of aircraft that can be profitably manufactured and sold. Generally speaking, the profit-loss break-even point of an aircraft project is around 200-300 units. With sales less than this number, the aircraft would not be competitive because of its high unit cost.

Therefore, an extremely important aspect of market and strategy research is to conduct a competition analysis of market share. It is a complete analysis and comparison of the design parameters of the new aircraft with those of similar aircraft that are already on the market or about to be introduced. The analysis is based on a combination of scientific methods and ad-hoc judgments. For example, suppose that by 1990 there is a demand for 1000 70-seat aircraft, and there are three similar aircraft competing for this market. First, a series of studies must be carried out to determine the unit cost, the cost of each passenger seat, the direct operating cost, and the feasibility and reliability of each aircraft. If the new aircraft designed for the 1990's can have one-third the market share, then the aircraft is considered viable, and the design and market survey can proceed until the aircraft is actually introduced on the market.

Development Strategy and Several Policy Questions

Determining the Number of Passenger Seats Is a Key Issue of Civil Aircraft Development Strategy

There are many different opinions and viewpoints on the strategy for developing civil aircraft; the most controversial question is concerning the number of passenger seats. This question should not be answered with haste, nor should a hasty decision be made based on opinions from a limited number of user organizations. We should first conduct a careful market research and base our decision on China's air transportation structure and needs.

Establishing Flexible, Multi-Form, Multi-Channel International Cooperation

Most of the mature aircraft types that are being produced today are products of international cooperation. Rarely is the entire production process carried out by one country or one manufacturer. The motivations for international cooperation are to increase economic benefits, to take advantage of maturing technologies, and to reduce cost. We must also adopt this flexible, multi-form, multi-channel cooperative approach so we can develop a mature civil aircraft which is comparable to the world standard and be able to establish a firm footing in China's market.

Establishing a Market Strategy Primarily Based on Domestic Market and Supplemented by International Markets

If the sales of an aircraft is limited to the market of only one country, it is difficult for it to reach the profit-loss break-even point; hence we

must consider developing foreign markets. However, without the support of domestic market, it is impossible to effectively develop foreign markets. Therefore, the market strategy should be primarily based on domestic market but supplemented by international markets, and we should develop these markets using a systematic and methodical approach.

China's Policy on Developing Civil Aircraft

After a rocky path of development over the past 30 years, China's civil aircraft industry is beginning to take shape. But even today the foundation of China's civil aviation industry is still weak and incomplete. The Ministry of Aviation Industry is facing a very serious question: how can we stimulate rapid growth of the civil aircraft industry? I believe that the development of civil aircraft is not merely the problem of a particular Ministry, it is an important indicator which reflects the standard and foundation of China's modern industrial capability; hence it deserves proper attnetion from the state. In order to guide civil aircraft development onto a healthy course, the state must establish the appropriate policy to protect and support the development. This policy should play an active and continuous role in raising the standard of the civil aviation industry and in cost reduction efforts. It should contain the following features: 1) allocate the necessary development funds; 2) include certain mature aircraft types in the national production plan; 3) provide favorable low-interest loans to the air transportation industry for purchasing Chinese-made aircraft. Within the forseeable future, it is impossible for China's civil aircraft industry to achieve healthy development without the supportive policy from the state. Therefore, the state's policy will play a deciding role as to whether China's civil aircraft development will succeed or fail.

Establishing a Complete Production, Sales, and Management System

The development of civil aircraft is a system engineering project. It must have a complete production, operation and management system which is compatible with China's current conditions. This system should break away from the traditional organization structures of the industrial ministries, and try to adopt the organizational structures of similar industries in other countries. In particular, it should contain such functional organizations as marketing, design, production and product support. In the areas of marketing and product support, we should establish operating procedures based on the development of today's international civil aircraft. This is the only way that China's civil aircraft development can become truly competitive.

I believe that as long as we set the correct course, establish a firm and stable policy, and have a good organization with sound management, the civil aircraft industry in China will have a promising future.

3012/12948
CSO: 4013/143

DESCRIPTION OF SHANGHAI PETROCHEMICAL COMPLEX NUCLEAR HEATING, POWER PLANT

Chengdu HE DONGLI GONGCHENG [NUCLEAR POWER ENGINEERING] in Chinese Vol 7, No 2, Apr 86, pp 1-7

[Article by Guo Zuodong [6753 0155 2629], Qian Jinhui [6229 6930 6540], and Liu Jukui [0491 5112 1145]]

[Text] I. Introduction

A significant fraction of the overall energy consumption is in the form of heat. Statistics show that in the United States, Japan, the Soviet Union and West Germany, the energy consumed in the form of heat is roughly 40 percent, 60 percent, 60 percent and 70 percent of the total energy consumption in each country. Figure 1 shows the total residential and industrial heat consumption in West Germany in 1977; it also shows that more than half the heat utilization is below 300°C.

Figure 1. 1977 User Heat Consumption and Temperature Distribution in West Germany

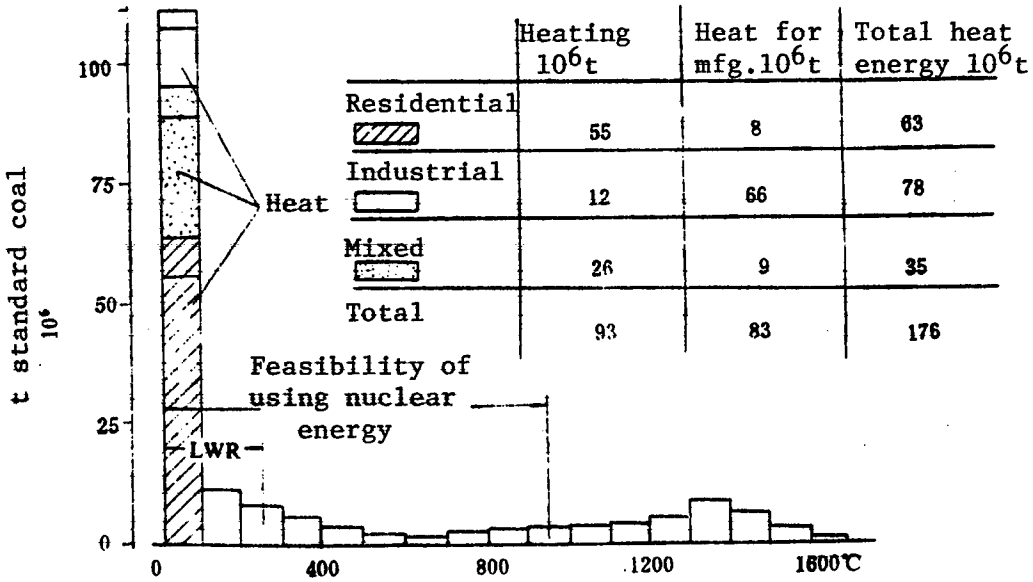

	Heating 10^6t	Heat for mfg.10^6t	Total heat energy 10^6t
Residential	55	8	63
Industrial	12	66	78
Mixed	26	9	35
Total	93	83	176

In China, the energy consumption in the form of heat in 1980 was approximately 400 million tons of standard coal. As more industries are developed and the people's standard of living is improved, finding an economic solution to the heat supply problem will become a major technical and policy question.

In conventional power plants, an economic way to utilize heat energy is to combine the production of heat and electricity. For example, in 1980 the coal consumption per kWh of electricity at the Beijing No 1 Heating and Power Plant was 20-30 percent lower than that of a pure electric power plant. This figure was based on a small generator unit; however, the same experience is expected to apply to nuclear power plants.

In other countries, nuclear reactors have been used for heat generation for over 20 years and are now being used for both industrial and residential heat supply. According to incomplete statistics, 52 heat-producing nuclear reactors around the world are under construction or have already been completed, and 16 are in the planning stage; most of them are combined heating and electricity nuclear power plants. The Soviet Union is currently the leader in this field; it has PWR nuclear power plants in the 1000MW class supplying heat to metropolitan areas. Experience from other countries also shows that nuclear heating and power plant is a cleaner source of energy than coal-fired heating and power plant. Figure 2 shows the 1976 consumption of primary energy sources in West Germany and the corresponding pollution level; it illustrates that industrial and residential heating not only consumes a large amount of energy resources, but is also the main source of environmental pollution. For this reason, the nuclear heating and power plant is potentially an attractive source of heat supply because of its economy and cleanliness. With increasing economic development and an improved standard of living, it will play an important role in the area of industrial heat supply and residential heating.

Figure 2.

Consumption of Primary Energy Resources and the Amount of pollutants Discharged in West Germany in 1976

Key:

A. consumption of primary energy resources
B. amount of pollutants discharged

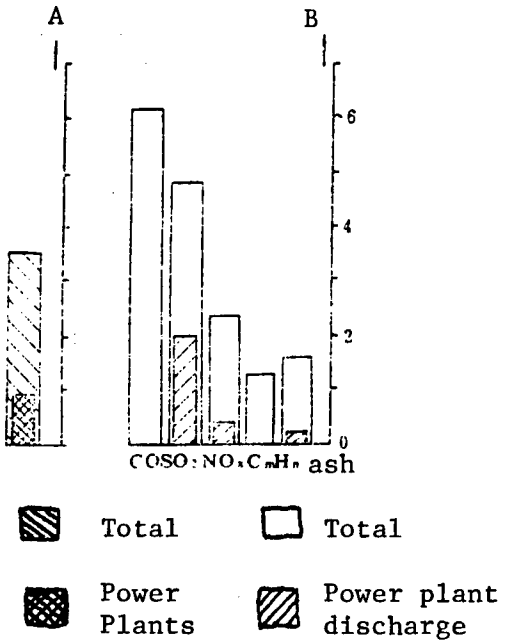

II. Design of the Shanghai Petrochemical Complex Nuclear Heating and Power Plant

Based on the experience of other countries, Chinese authorities in 1981 suggested the possibility of replacing petroleum with nuclear fuel. To study this issue, we have initiated an effort to develop a small-scale nuclear reactor for the combined production of heat and electricity, and to use it to supply heat to petrochemical plants; specifically, we conducted a feasibility study of developing such a reactor for the Shanghai Petrochemical Complex. Based on the heating load of the Complex and the corresponding electricity output, we estimated the single reactor thermal power to be 450MW, and proceeded with the reactor design. The Shanghai Petrochemical Complex is built on the beach of Hangzhou Bay where the soil structure is very soft, and the base rock is 180 meters deep. Hangzhou Bay is a densely populated region and is also an important fishing port; the local chemical industry imposes strict requirement on the reliability and safety of the heat supply system. Furthermore, the heat supply unit must be located close to the heat load center, which considerably limits the site selection of the power plant. Because of these special requirements and the technical complexity of the nuclear heating and power plant, the feasibility issue cannot be addressed by conventional means; a preliminary design must first be carried out before conclusions can be drawn about these special problems. For this reason, a 3000 man-month effort was initiated, which included thorough investigations, overseas tours, consultation with foreign experts. Also, special conferences were held where Chinese experts were invited to discuss problems of environmental protection, safety of the steam supply system, design specifications, foundation treatment at the plant site and equipment supply. Finally, a feasibility report was issued.

1. Design Summary

Based on China's current nuclear power technology and available information from other countries, a pressurized-water reactor (PWR) design is selected for this heating and power plant. For reasons of environmental safety, a double-layered shell structure is used to provide extra protection; a three-circuit design is selected for the steam supply system to guard against radiation hazards; also, two reactors are connected for parallel operation to ensure the reliability of the steam supply.

A flow diagram of the system is shown in Figure 3.

The heat carrying system consists of the reactors, the steam generators and the main pumps connected by the main pipes. This system has two separate circuits, each circuit contains a steam generator and a main pump; both circuits share the same pressure stabilizer. The operating pressure in the No 1 circuit is 150 kg/cm^2, the coolant flow rate is 12,000 tons/hr, the exit water temperature from the reactor is 307.5°C, and the inlet water temperature is 282.5°C. Under rated power load conditions, the steam pressure in the No 2 circuit is 50 kg/cm^2, and the temperature is 262.7°C (saturated). The temperature of the water supply from No 2 circuit is 205°C, and the steam output from each reactor is 836 tons/hr. By using the steam in the No 2 circuit as a heat source, two secondary evaporators are used to produce medium-pressure steam (35 kg/cm^2

saturated steam) at a rate of 75 tons/hr. By using intermediate bleed gas from the high-pressure tank of the steam turbine as a heat source, 15 kg/cm^2 saturated steam is produced from a heat exchanger at a rate of 320 tons/hr. In addition, each reactor is capable of generating approximately 60,000 kW of electricity.

Figure 3. System Flow Diagram of the Nuclear Heating and Power Plant

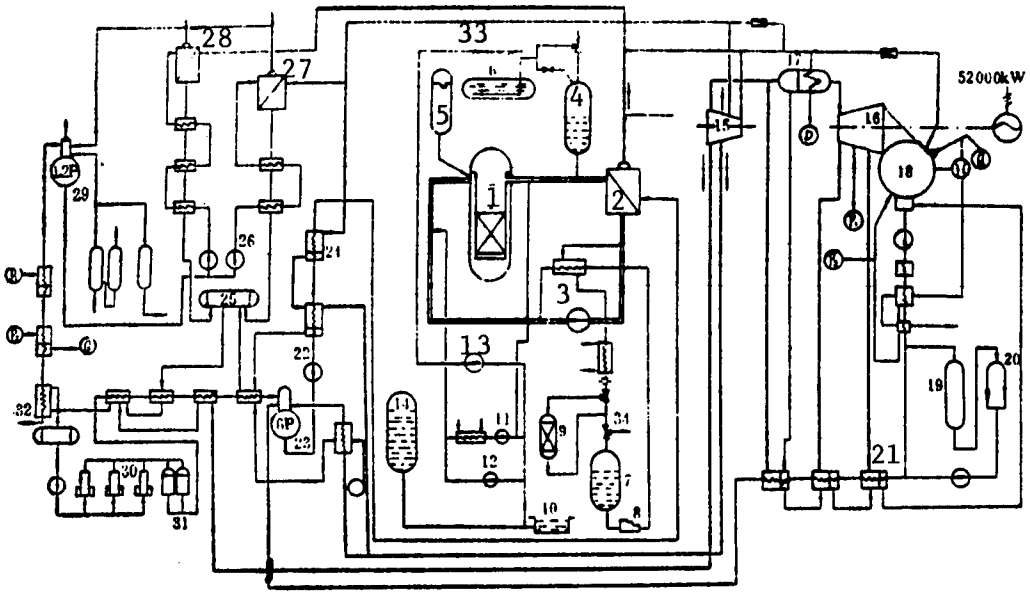

Key:

1. reactor
2. steam generator
3. main pump
4. pressure stabilizer
5. safety injection tank
6. pressure relief tank
7. volume control tank
8. top filling pump
9. resin bed
10. safety shell pit
11. reactor shut-down cooling pump
12. safety injection pump;
13. spraying pump
14. refueling water tank
15. high-pressure turbine
16. low-pressure turbine
17. reheater for steam/water separation
18. condenser
19. hydrogen ion exchanger
20. mixing bed
21. low-pressure heater
22. main water supply pump
23. high-pressure de-oxidizer
24. high-pressure heater
25. water collection tank
26. relay pump
27. low-pressure de-oxidizer
28. medium-pressure evaporator
29. low-pressure de-oxidizer
30. electromagnetic filter
31. mixing bed
32. three-circuit auxiliary water supply
33. safety shell spray system
34. to boron return system

According to the design load factor, this proposed nuclear heating and power plant can produce 533 million kWh of electricity and 3.085×10^{12} kcal of heat annually, which is equivalent to 439,000 tons of oil. Its thermal efficiency can reach 70 percent, which is double the thermal efficiency of conventional nuclear power plants.

The reactor core has 45 17x17 standard fuel elements, which contain three different concentration levels of ^{235}U: 1.8 percent, 2.4 percent, and 3.1 percent; the equilibrium refueling concentration is 3.4 percent. Each reactor is loaded with 17.232 tons of fuel, and the refueling cycle is 300 full-power days. The average burnout is 27,000 MW.D/TU, and the maximum burnout is 43,000 MW.D/TU.

Figure 4 shows the main reactor room. The inner shell is made of steel; the inner diameter is 29 m, the cylinder wall thickness is 32 mm, the overall height is 57 m, and the net volume is 25,000 m^3. The outer shell is made of cement; its inner diameter is 31.864 m, the wall thickness is 0.7 m, and the overall height is 59 m.

Figure 5 and Figure 6 show the layout of the main and auxiliary reactor rooms of the nuclear island. It is designed so that the two reactors are located close to each other and share the same nuclear fuel depot; also, the main control room and the electric room are located above the auxiliary reactor room.

Figure 4. Main reactor room

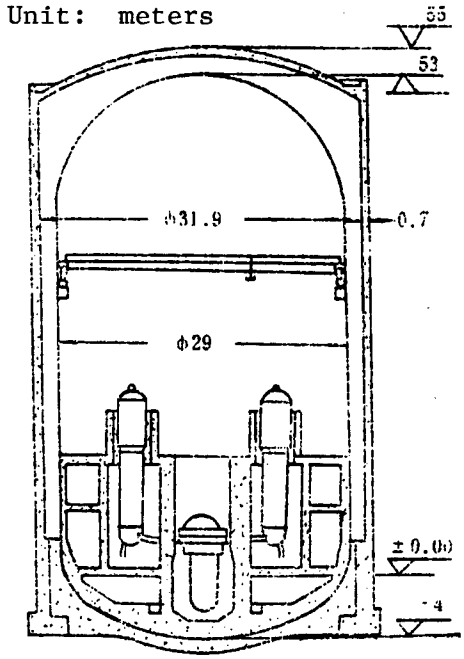

Figure 5.

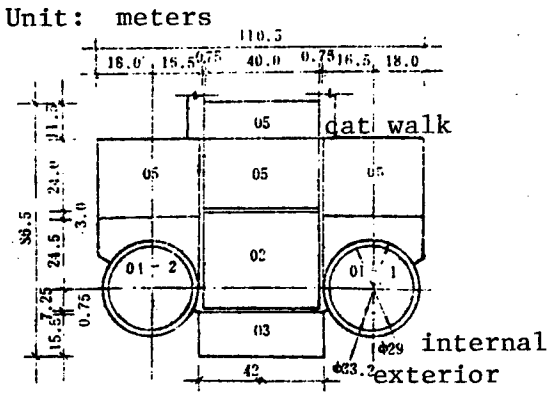

2. Design Features

(1) The Reactor is Sufficiently Safe to be Built in a Densely Populated Region

In order to locate the reactor near heavily populated load centers while meeting the requirements of the national safety regulations, the following measures have been taken: 1) installation of the double-layered safety shell; 2) improvement of the gas removal process.

Figure 6. Cross Sectional View of the Nuclear Island

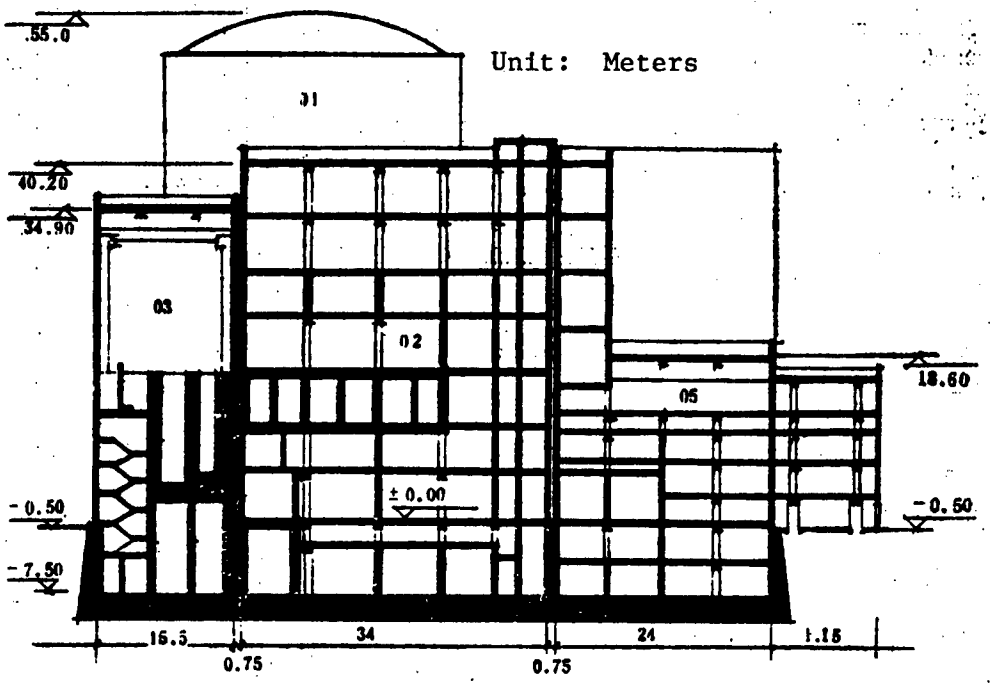

Calculations show that it is safe to build the reactor in a residential district with a 500 m perimeter around the proposed plant site. Under normal operation, the maximum radiation dosage per person at the perimeter of the plant site is only 0.0912 millirem, which is 0.18 percent of the allowable dosage of 50 millirem specified in the national radiation protection regulation (GBJ-8-74). Even in a purely hypothetical accident where the main pipes broke at both ends, causing loss of water and reactor core melt-down, there is still no need for emergency evacuation of residents outside the perimeter of the plant. The calculations also show that under the most unfavorable weather conditions, the population dosage over a wide region 30 days after the accident is quite low. To verify this result, we have submitted the data to the U.S. Nuclear Regulatory Commission, which agreed with our calculations and considered the results to be conservative. Therefore, it is safe to conclude that building this proposed power plant in a densely populated region is consistent with current regulations.

In order to further reduce the effect of radioactive gas on the environment, we have installed a gas removal system in the No 1 circuit, and used the volume control tank for continuous gas sweeping in place of the gas removal tower of the boron return system; this leads to simpler operation and increased safety.

(2) The Reactor Control Design Leads to System Simplification and Meets Advanced Technical and Economic Standards

This reactor has 21 control rod elements, which is 47 percent of the reactor core fuel elements. They provide sufficient control capability so that regulating the boron concentration level is not required. Instead, the new

technique of rod control with boron burnout compensation is used, which greatly simplifies the system design, improves the safety, efficiency and reliability of the power plant, and also simplifies operation. The basic features of this system are as follows: A) The chemical container system is only used for compensating reactor core burnout and for achieving hot starting below the iodine pit. During steady, full-load operation, the regulating rod is removed from the reactor core to achieve more uniform power and deeper burnout. Below the iodine pit hot starting can be achieved by diluting the boron level and lifting the regulating rod without waiting for tritium decay. B) Both cold and hot starting are accomplished by rod control. Reactor shutdown or starting requires no boron regulation; it is only required for refueling or cold start. In this way, if the main steam pipe breaks, re-inserting the control rod can prevent the reactor core from returning to the critical state without emergency boron injection.

The starting operation is simpler and safer; when the temperature of the No 1 circuit rises to 100°C, because of the negative temperature coefficient, nuclear reaction can be used to accelerate the starting process, thus raising the load factor of the power plant.

The design volumes of the boron return system and the waste water system can be reduced in order to simplify the system and to reduce cost. The concentration level of the boric acid is decreased in order to eliminate the cumbersome heating system for concentrated boron.

The above control system not only can maintain uniform power distribution, it also reduces the amount of waste water discharge; consequently, the safety, economy and reliability of the power plant are improved.

(3) Higher Thermal Efficiency.

A reasonable heat to electricity ratio is selected for the power plant to achieve higher thermal efficiency. To accommodate the different heat supply loads of the Shanghai Petrochemical Complex between winter and summer, this reactor can change its operating mode so that thermal efficiency can vary from 68.7 percent to 78.9 percent; the average thermal efficiency is higher than 70 percent.

(4) Construction for Soft Soil Foundation.

After repeated comparisons and consultations with the construction departments, a pile foundation design with box support was chosen to overcome the difficulty of building on soft soil.

III. Construction Cost and Economic Considerations

Because this nuclear heating and power plant must be located near a factory, must have high safety standards, and is to be built on soft soil foundation, the construction cost is rather high. After careful discussions and reviews with the construction, assembly and equipment supply units, and taking into account various uncertain cost factors, the cost of the construction project

was estimated to be 702.35 million yuan (which includes nearly 80 million yuan for treatment of softsoil foundation). The total cost including initial fuel cost, preparation cost and design review cost will be 873.8 million yuan. This figure closely approximates the cost of building the 300 MW Qinshan nuclear power plant, and therefore is considered to be a reliable rough estimate.

On the basis of this estimate and a 6-year construction period, we have calculated the cost of heat and electricity production based on the current interest rate and capital retrieval period. The result is compared with the costs of oil-burning and coal-burning power plants, as shown in Figure 7.

Figure 7. Production Costs of Three Different Heating and Power Plants for the Shanghai Petrochemical Complex

Note: head supply unit production cost (yuan/kcal) x 3.085×10^{12} kcal + power generation unit production cost (yuan/kw-hr) x 533 million kw-hr

Key:

1. oil-burning power plant with high-priced oil
2. current oil price plus tax
3. nuclear heating and power plant
4. coal-burning power plant with current coal price
5. coal-burning power plant with 1990 price level
6. coal-burning power plant with export coal price
7. coal-burning power plant with export coal price and sulfur removal

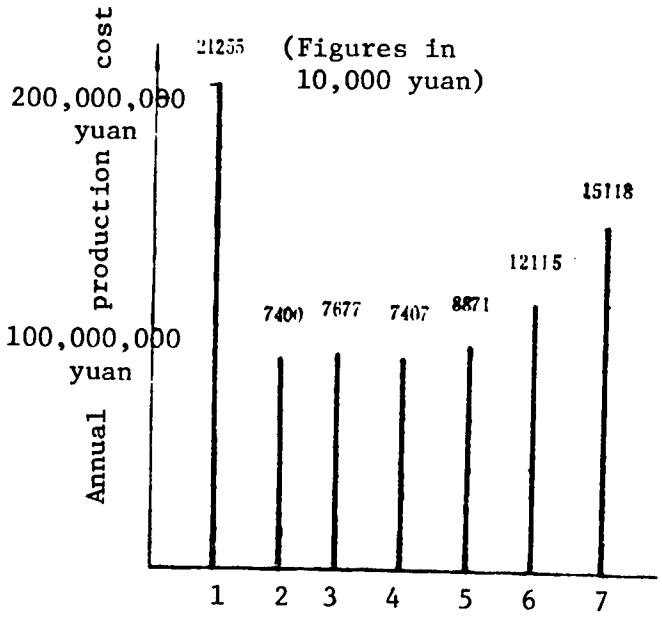

It can be seen from Figure 7 that the cost of heat and electricity production of this nuclear power plant is essentially the same as the cost based on current oil price or the equivalent heavy oil price plus oil-burning tax. But compared with the 1990 price level, there is a distinct difference because the nuclear fuel remains flat whereas coal price continues to rise. The economy of nuclear power plant is better than current coal-fired power plant if sulfur removal is included in the current coal price. The main disadvantages of the nuclear heating and power plant are the high initial construction cost, the long construction period and delayed economic payback.

IV. Key Issues for Improving Economic Benefits and Competitiveness

This nuclear heating and power plant is designed to have all the components that a large nuclear power plant has except they are smaller in size. This is

a low risk approach because only mature technology is used. But there is one serious drawback, i.e., the scale of construction has not been reduced in proportion to the reduction in reactor power. As a consequence, there are a number of adverse effects such as high construction cost, long construction period and delayed economic payback. In order to improve its competitiveness, we must try to reduce the scale of construction and increase the construction speed without sacrificing safety. A small-scale nuclear power plant can only survive if its construction cost is lower and its construction period is shorter. In this design, we have taken the following exploratory measures to achieve this goal:

1. Use of Compact Layout in Designing the Nuclear Island

Figure 8 shows a comparison of the cost of power generation between the French CAS-3G small-scale nuclear power plant and the oil-burning power plant for different power levels. The relationship between the basic construction cost and the plant capacity also follows a similar trend. Figure 9 shows the relationship between different types of layout and the size of the safety shell. In the case of the Qinshan nuclear power plant (728), the dimensions correspond to the outer dimensions of the concrete shell; in the case of CAS and NP, they correspond to the dimensions of the steel shell. It is shown that the safety shell is much smaller if a compact layout is chosen. On the basis of this design groundrule, the safety shell of this power plant can be reduced by 9 m to less than 20 m. This will result in considerable reduction of the scale of construction, and thus lower construction cost and faster construction speed.

Figure 8. Comparison of the Cost of Power Generation Between the French CAS-3G Nuclear Power Plant and Oil-Burning Power Plant

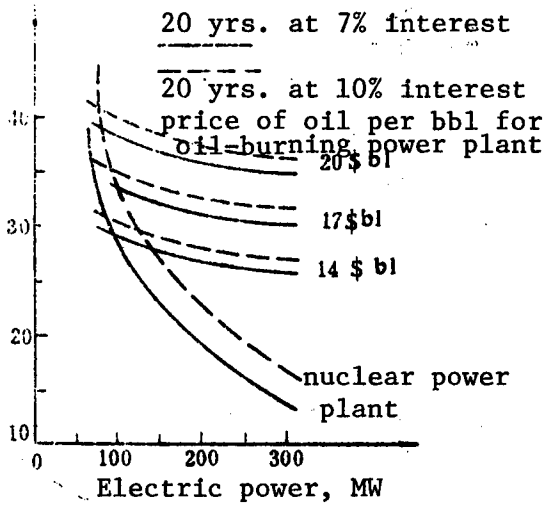

Figure 9. Effect of Different Layout on the Size of Safety Shell

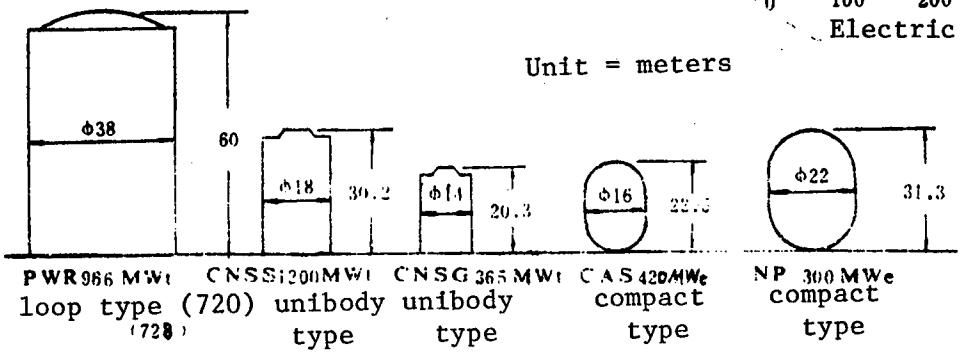

2. System Simplification

With the nuclear island reduced in size, the system should be simplified accordingly in order to reduce the size of the auxiliary building. The previously described control technique which uses rod control with boron compensation is highly complicated. Analysis shows that on a small reactor, it is feasible to use solid poison for control without boron; but to implement this technique requires experimental verification. Eliminating the use of boron will reduce the number of valves and simplify the system; it will also reduce the amount of waste material and ultimately reduce the size of the auxiliary building. Hence this is a significant improvement.

3. Lowering the Nuclear Fuel Cost

Economic analysis shows that the price of nuclear fuel approaches a sensitivity of 60 percent in the cost structure. Therefore, another aspect of increasing the competitiveness of small nuclear heating and power plant would be to increase the accuracy of physical calculations, improve the performance and lowering the price of fuel elements.

4. Improving Quality Management

In order to ensure that the nuclear power plant will have high load factor, we must try to improve the quality management during design and construction. Figure 10 shows the relationship between the cost of heat supply and the number of yearly operating hours of a West German low-temperature nuclear reactor. They believe that to achieve low heat-supply cost, the reactor must operate more than 6,000 hours annually, otherwise the economic payoff would be much lower.

An economic analysis of the Shanghai Petrochemical Complex Nuclear Heating and Power Plant shows that if the load factor decreases from 70 percent to 50 percent, then the cost of power generation and heat supply will increase by 22 percent. Therefore, an important design consideration is to try to improve the operating reliability and annual load factor of the nuclear and power plant.

Figure 10.

Relationship Between Cost of Heat Supply and Number of Hours of Annual Operation for West German Low-Temperature Heat Supply Reactor

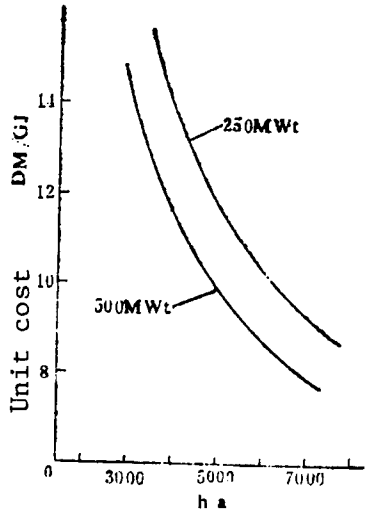

5. Standardization and Other Issues

By emphasizing standardization and carrying out fabrication and assembly in the factory as much as possible, the amount of labor in the field can be minimized, thus improving quality control and increasing the speed of construction.

Through feasibility studies, we have acquired a fairly complete understanding of small-scale nuclear heating and power plants. We believe that 800 million yuan will be approximately the upper limit of the construction cost. The cost can be reduced by implementing any one of the improvement measures described above. Furthermore, this is the first nuclear heating and power plant for which all components are produced on a single-unit basis. It is expected that the construction cost will drop below 800 million yuan after a number of reactors have been built, and then such power plants will become more competitive.

3012/8918
CSO: 4008/76

450MW PWR FOR JINSHAN NUCLEAR HEAT, POWER PLANT

Chengdu HE DONGLI GONGCHENG [NUCLEAR POWER ENGINEERING] in Chinese Vol 7, No 2, Apr 86, pp 8-10

[Article by Shen Lubing [3088 1462 0393]]

[Text] I. Introduction

The nuclear heat and power plant of the Shanghai Petrochemical Complex is powered by a pressurized-water reactor (PWR) which uses light water for cooling and moderation. This type of reactor is the most widely constructed and operated reactor in the world; it is also a reactor with proven safety and economy. The reactor is composed of a pressure vessel, a reactor core, internal structural components and sensing devices, and drive mechanism (Figure 1). It has a maximum diameter of 3,260 mm, overall height of 13.7 m, and a dry weight of 213 tons. The design thermal power of the reactor is 450 MW, the coolant pressure is 150 kg/cm^2, the inlet temperature is 282.5°C, the exit temperature is 307.5°C, and the total flow rate is 12,000 tons/hour.

The reactor has two separate circuits: the coolant enters the pressure vessel from the inlet pipe, passes through the annular cavity between the vessel and the hanging basket, and flows down to the bottom of the vessel; then it makes a 180° turn through the flow distribution skirt and the flow distribution plate into the reactor core; carrying away the heat produced in the core, it finally flows outside through the two exit pipes. Approximately 5 percent of the total coolant flow is used to cool the cover of the pressure vessel, the heat screen of the hanging basket, and the control rod.

The reactor design streese safety, practical utility, economy and the use of advanced technology. Its main features are as follows:

1) Standard 17x17 fuel elements are used in order to promote compliance of Chinese-made fuel elements with international standards, and to facilitate the use of foreign technology and experience.

2) The pressure vessel is reinforced using integral pipe connections. The exit and inlet pipes are both of the seated type which has a shorter weld seam; therefore, it facilitates the manufacturing process such as welding and flaw detection.

Figure 1.

Structure of the 450MW Reactor

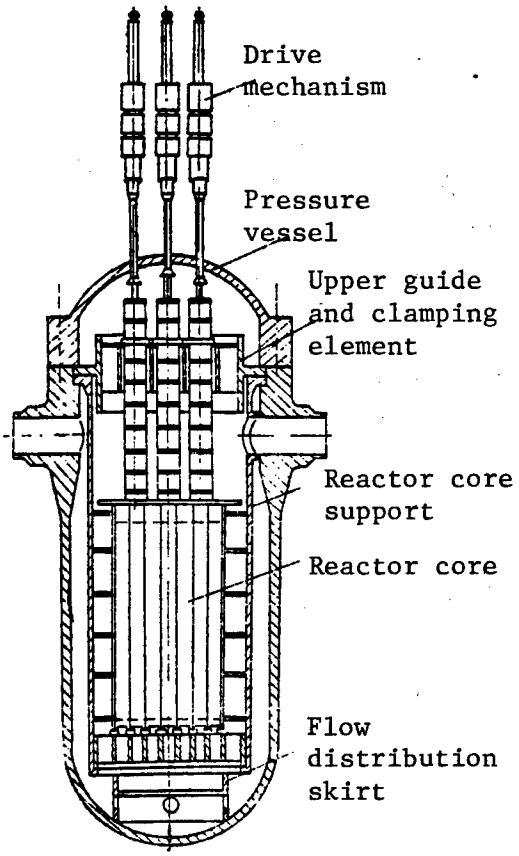

3) The pressure vessel has no other connecting pipes below the main coolant pipe; hence if a crack develops in the connecting pipe, the reactor core will be submerged by water from the emergency cooling system.

4) There is a large annular water cavity between the pressure vessel and the hanging basket, which is designed to keep the integrated neutron flux (E> 1MeV) inside the vessel over a 40-year period to be less than 1.61×10^{19} n/cm^2, and to provide protection against accidents due to loss of water.

5) The reactor has two safety injection tubes which extend to the lower part of the reactor core. In case of water loss, emergency water can be quickly supplied to the reactor via the safety injection tubes.

6) All support plates inside the reactor are made of welded components. The compressing spring consists of a small butterfly spring element; this design eliminates the use of bulky stainless-steel forged parts, and can be fabricated totally in this country.

7) The neutron flux in the reactor is measured by a vanadium-ball detection system.

8) Both rod-control and boron-control techniques are used to regulate the nuclear reaction; during normal operation, only rod-control is used for starting and stopping the reactor.

II. Pressure Vessel

The pressure vessel consists of two main sections: the cylindrical body and the top cover. The two sections are connected by flanges with two "O" rings in-between and pressed against one another by 44 sealing bolts. The vessel is 8284 mm tall, has a maximum diameter of 3260 mm and weighs approximately 124 tons.

The cylinder has an inner diameter of 2700 mm and a wall thickness of 135 mm; it is a welded structure consisting of a seamless forged bottom enclosure, a cylindrical shell and a cylindrical flange.

The flange has four coolant connectors and two safety injection connectors; the flange thickness satisfies the reinforcement requirement of the connectors. This integral flange design with reinforced connectors not only eliminates a main weld seam on the cylinder, but also simplifies the welding process and reduces the amount of solder flux required, thus improving the stress condition in the connector region.

The top cover consists of a forged flange welded to a spherical cap. The spherical cap has 21 connectors for the drive mechanism, 6 connectors for the sensor ports and 1 connector for the exhaust port. The reinforcement of these connector ports is accomplished by uniformly increasing the thickness of the spherical cap.

The rpessure vessel is made of fine-grain ASTMSA508-3 steel, which has very good properties under neutron radiation.

The inner surface of the pressure vessel is covered with a layer of Austenite stainless steel; the outer surface has a layer of metallic reflecting type thermal insulation.

III. Reactor Core

The reactor core consists of 45 fuel elements and 21 control rods; its equivalent diameter is 1.63 m and its height is 2.73 m. The rather large height-to-diameter ratio of 1.68 results in poor neutron efficiency, but it reduces the capacity of the main pump and the diameters of the pressure vessel and the main pipes. This design is chosen primarily in consideration of China's manufacturing capability of reactor components even though certain physical performance may be sacrificed. Calculations show however, that the average equilibrium burnup level can still reach 27,000 MW·D/TU.

The initial fuel elements of the reactor core has three concentration levels: 1.8 percent, 2.4 percent, and 3.1 percent; the equilibrium refueling concentration level is 3.4 percent. In addition, burnable poison rods made of 272B4C-Zr-2 material are installed inside the reactor so that the radial coefficient of power non-uniformity is kept below 1.499, and the axial coefficient is 1.735. After considering the effect of local power peaks and computational errors, the overall coefficient of power non-uniformity is estimated to less than 2.81. The thermodynamic design calculations show that under normal operating conditions, the minimum burnout ratio of a typical channel is 2.62, and

the maximum temperature of the core block is 1744°C; the minimum burnout ratio under 118 percent overload condition is 2.16, and the maximum temperature of the core block is 1949°C.

The reactor core has 21 control rod elements which are inserted in 47 percent of the fuel elements; they provide sufficient control capability for starting or shutting down the reactor without boron dilution or addition, thus considerably simplifying the boron return system. The control rods are divided into 2 categories: one is called the shutdown rod unit which has 13 elements separated into 3 groups S_1, S_2, S_3, all made of Ag-In-Cd absorbing material; the other is the gray-body regulating-rod unit, which has 8 elements separated into 2 groups R_1, R_2, it has 8 Ag-In-Cd rods and 16 stainless-steel rods.

The fuel elements are arranged in a standard 17x17 array, which essentially has the same structural form, dimensions and fuel concentration level as the fuel elements of the Guangdong Nuclear Power Plant imported from France; the only differences are: (1) the overall length of the elements is reduced to 3,088 mm, and the total weight is 498.8 kg; (2) the elements contain no special instrument guide tubes; (3) the enclosure material is made of annealed Zr-4 tubes rather than cold-quenched tubes, and the thickness of the enclosure shell is increased from 0.57 mm to 0.64 mm in order to imporve the reliability of the first layer safety shield.

The reactor also contains such components as the burnable poison elements, neutron source elements and flow stops.

IV. Structural Members Inside the Reactor

The structural members inside the reactor include the reactor core support structure, the upper flow guide and clamping unit, and the flow distribution skirt. Their main functions are to support and position the fuel elements, the control rods, and the sensing elements, as well as to properly guide the coolant flow inside the reactor.

The reactor core support structure weighs approximately 31 tons, stands 5,667 mm, and has a maximum diameter of 2,540 mm. The structure consists of the handing basket, the heat shield, the enclosure plate, and the lower support plate; the entire structure is suspended onto the pressure vessel flange through the flange of the hanging basket cylinder, and is properly aligned by 4 position pins. During inspection of the pressure vessel, the structure can be lifted out as a single unit.

The upper flow guide and clamping unit weighs 13.5 tons, stands 2840 mm and has a maximum diameter of 2,540 mm; it consists of 21 flow guide elements, 21 support columns, 1 upper support plate and 1 lower lattice plate. The support column not only links the upper support plate and the lower lattice plate into a single structure, it also protects the flow guide from being bombarded by the water flow; in particular, it ensures that the flow guide continue to function during a loss-of-water accident. The upper flow guide and clamping unit is attached to the flange of the hanging basket through the flange of the upper support plate, and presses tightly against the top cover of the pressure vessel.

The design of the structural members takes into account such factors as fabrication procedures, cost and domestic manufacturing capability; for example, the upper and lower support plates are made of welded frame structures instead of large forged parts, the large compressing springs are replaced by small butterfly spring units.

V. Sensing Elements Inside the Reactor

The reactor has six sensing units which include the wiring box, the finger-shaped lead-in tubes and the main lead-out tube. The wiring box contains the pneumatic-ball guide tube, thenitrogen tube and the thermocouple and electric cables, and feeds them through the main lead-out tube to the outside of the reactor; it also distributes the finger-shape lead-in tubes to the various sensor locations in the reactor core. Each sensing element may be connected to 2 or 3 lead-in tubes. A lead-in tube consists of a ball sensing tube and a thermocouple. The sensing units are located on top of the upper support plate, between the flow guide units; they can be lifted out during refueling and kept in a water container. This design greatly facilitates maintenance and repair and simplifies replacement procedure.

VI. Drive Mechanism

The drive mechanism performs the function of regulating the movement of the control rods. In this reactor, a magnetic lifting drive mechanism is used in which two locking hooks can operate the control rods through the drive linkages; the locking hooks are activated by energizing or de-energizing three excitation coils according to a preprogrammed sequence.

The mechanism includes the executive segment, the pressure bearing segment, and the position indicator. The executive segment consists of three operating coils, three magnets and armatures, the locking hooks and the drive linkages; for each magnet there is a corresponding armature. The pressure shell is located between the three coils and the three magnets; it provides a pressure boundary for coolant, and separates the mechanical from the electric segment. The position indicator is composed of an independent position indicating coil which fits over the travel tube of the drive linkages; there is a coil at each of the top and bottom end of the travel tube to indicate the position limits. The design travel of the mechanism is 2,630 mm, the step size is 10 mm, and the normal lift load is 80 kg.

3012/8918
CSO: 4008/76

NUCLEAR CORE DESIGN OF 450MW PWR

Chengdu HE DONGLI GONGCHENG [NUCLEAR POWER ENGINEERING] in Chinese Vol 7, No 2, Apr 86, pp 11-16

[Article by Wang Chengji [3769 2110 1015], Cai Yucai [5591 3768 2088], Zhang Zhongyao [4545 1350 5069], Xu Xiufang [1776 4423 5364], Wu Yinxian [0702 1714 0103], Ma Qingsheng [7456 1987 3932], and Liu Jingbo [4091 7234 3134]]

[Text] I. Introduction

The objective of nuclear core design is to design the initial core layout, the mode of reactor control and the mode of refueling in order to satisfy the requirements of 450MW of rated heat power output and the 300-day refueling cycle. Specifically, it provides the basic data for the starting, safe operation, shut-down and refueling of the reactor; it also provides design guidelines for reactor thermodynamics, shielding and control. In addition, it will establish the necessary measures to achieve uniform power distribution, to increase the power density and to increase the burnout depth of the reactor core in order to meet the safety and economic requirements of the nuclear heating and power plant.

1. Physical Design Guidelines of the Reactor

a) Under full load conditions, the overall coefficient of power non-uniformity of the reactor core must be less than 3.

b) From zero to full load, the temperature coefficient of the moderator must be negative.

c) Under normal operating conditions, reactivity control will be accomplished by a hybrid technique of rod control and boron regulation; during reactor starting or shut-down, reactivity control will primarily rely on the control rods.

d) Under any operating condition, if the control rod module with the highest efficiency is stuck outside the reactor core, the remaining control rod modules will be able to execute cold and hot shut-down.

e) Under equilibrium fuel circulation conditions, the maximum burnout depth of the unloaded fuel module must not exceed 50,000 trillion Watt-day/ton Uranium.

2. Layout of Reactor Core

The reactor core consists of 45 fuel modules, each module contains 265 fuel rods and 24 guide tubes (for locating the control rods, burnable poison or internal sensors), which are arranged in a 17x17 square array. The height of the reactor core is 273 cm, and the equivalent core diameter is 162.74 cm. The reactor core is divided into 3 loading zones whose initial concentration levels are respectively 2 percent, 2.4 percent and 3.1 percent; there are 13 modules with concentration level of 2 percent and 16 modules each with concentration levels of 2.4 percent and 3.1 percent. The modules are separated by a distance of 21.5 cm.

The reactor has 21 bundles of control rods which are divided into two types: one type is made of silver-indium-cadmium alloy and is used for reactor shutdown, each bundle consists of 24 rods; the other type is used for regulation, and each bundle consists of 8 silver-indium-cadmium rods and 16 stainless steel rods. There are 13 modules of the former type and 8 modules of the latter type. In addition to the control rods, boric acid solution is added to the moderator to provide effective control. In order to avoid excessive boron concentration which may lead to positive temperature coefficient of the moderator, 272 pieces of burnable poison (B_4C-Zr-2) are placed in the initial loading of the reactor core. The layout of the reactor core is shown in Figure 1.

Figure 1.

Layout of the Reactor Core

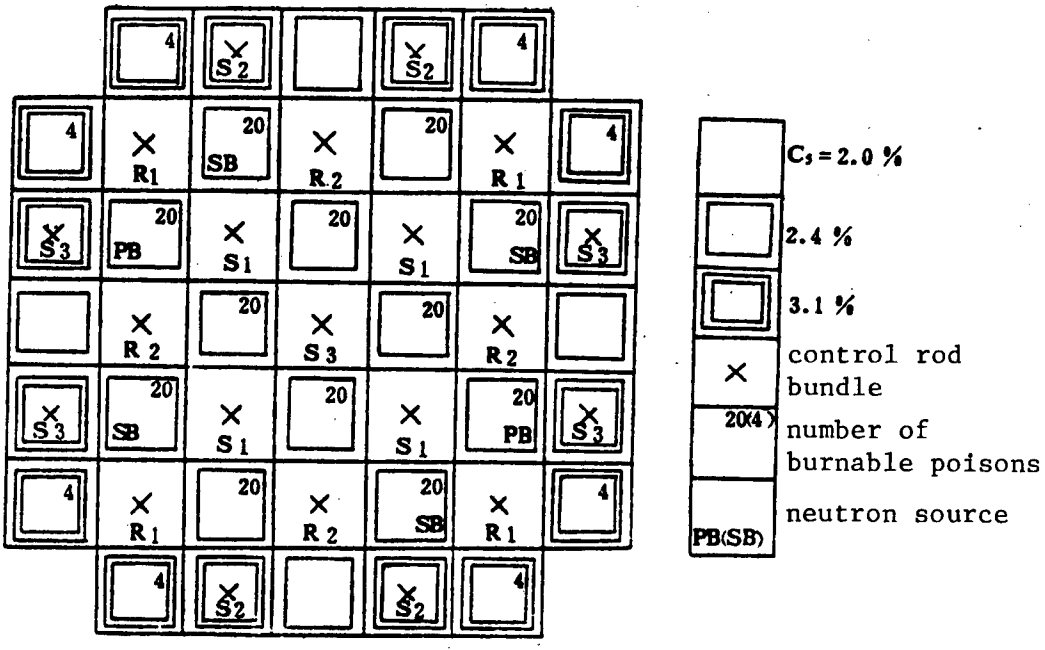

3. Key Parameters of the Reactor Core

rated heat power, MW	450
operating pressure, kg/cm^2	150
reactor height, cm	273
average volumetric power density, W/cm^3	79.2
average linear power density, W/cm^3	138.2
hot-state zero-power coolant average temperature, °C	278
hot-state full-power coolant average temperature, °C	295
average fuel concentration, %	3.4
total uranium dioxide loading, tons	17.232
zone 1 U-235 loading, kg	86.766
zone 2 U-235 loading, kg	129.622
zone 3 U-235 loading, kg	167.427
total U-235 loading, kg	384.815
burnable poison B-10 loading, g	566.3
volumetric ratio of water to uranium dioxide	1.96
number of guide tubes in each module	24
number of fuel element rods in each module	265
diameter of fuel element rod, mm	9.5
core diameter of fuel-element rod, mm	8.05
thickness of fuel-element rod, mm	0.64
material of fuel element enclosure	Zr-4
core density of uranium dioxide	94% theoretical density
burnable poison material	B_4C-Zr-2
density of burnable poison, g/cm^3	6.267
outside diameter of burnable poison, mm	9.5
inside diameter of burnable poison, mm	8.1
linear density of boron, g/m	0.7626
total number of burnable poison	272
control rod diameter, mm	9.7
absorber diameter, mm	8.62
control rod enclosure material	S.S
control rod enclosure thickness, mm	0.54
moderator temperature coefficient, pcm/°C	-13.4 to -47.4
fuel temperature (Doppler coefficient, pcm/°C	-2.55 to -2.32
power coefficient, pcm/1 % p	-12 to -17
effective percentage of latent neutrons, %	0.007049
neutron life, μs	18.71
strength of neutron source (PO-Be source 2), n/s	$1x10^8$
strength of neutron source (Sb-Be source 4), n/s	$0.5x10^8$

II. Distribution and Control of Residual Reactivity

1. Distribution of Reactivity of the Initial Life Cycle

The total residual reactivity of the reactor core is the reactivity of a cold-state, clean reactor at the beginning of life. It is determined by the fuel loading, the concentration level, the water-to-uranium volumetric ratio, and the structural material. It directly affects the cycle life of the reactor core and the burnout depth. The distributions of reactivity have been computed based on the k_{eff} values listed in Table 1 for different conditions; the results

Table 1. Effective Multiplication Factor k_{eff} for Different Conditions at the beginning of Life and End of Life of the Initial Cycle

Condition of reactor core					
Beginning of life	Cold state	Without ^{135}Xe, ^{149}Sm, FP	Without solid boron	Without control rod	1.277262
Beginning of life	Hot-state zero-power	Same as above	Same as above	Same as above	1.22594
Beginning of life	Hot-state full-power	Same as above	Same as above	Same as above	1.202971
End of life	Hot-state full-power	Same as above	Same as above	Same as above	1.107571
End of life	Same as above	With ^{135}Xe, ^{149}Sm, FP	Same as above	Same as above	1.012149
End of life	Same as above	Same as above	With solid boron	Same as above	1.0
End of life	Same as above	With ^{135}Xe, without ^{149}Sm, FP	Same as above	Same as above	1.062243
End of life	Same as above	Without ^{135}Xe, with ^{149}Sm, FP	Same as above	Same as above	1.027092

are presented in Table 2. It is shown that two thirds of the total residual reactivity is used to compensate for the reactivity losses caused by various effects; the reactivity loss due to fuel burnout is only one third of the total residual reactivity, $\Delta k_{eff}=0.0954$.

2. Control of Core Reactivity

Compared with typical pressurized-water reactors that exist today, significant improvements have been made in the mode of reactor core control of nuclear heating and power plants. The 21 bundles of control rods have sufficient control capability to provide reactor power regulation, compensation of xenon poison reactivity effect and cold and hot reactor shut-down; the boric acid in the reactor core coolant is primarily used to compensate for the slow variation in reactivity of fuel burnout and to control reactivity during refueling and cold shut-down. Thus, the reactor has two independent shut-down systems which ensure the safety of shut-down and refueling operations. The solid control rod system reduces the requirement of boronization and dilution of the chemical container system, and therefore reduces the amount of waste water to be treated by the boron return system. It has been proven that accidents of broken main steam pipes can be prevented by eliminating the high-concentration boron system. As a result, the boron return system and the safety injection system are greatly simplified. Based on preliminary estimates, the equipment costs of the chemical container system and the boron return system can be reduced by 30 percent and 45 percent respectively, and the building space of the auxiliary buildings will also be greatly reduced.

The results of control calculations under different conditions of the initial clean reactor are presented in Table 3.

3. Grouping of Control Rods and Their Values

There are two groups of control rods: R_1, R_2, each group contains 4 bundles. There are three groups of shut-down rods: S_1, S_2, S_3; S_1, S_2 each contains 4 bundles and S_3 contains 5 bundles. The layout inside the reactor is shown in Figure 1. When R_2 is the primary regulating group, R_1 becomes the secondary regulating group. Table 4 lists the composite values of each rod group under hot-state at the beginning of life and end of life. Under the condition of hot-state full-power without xenon, the differential values of the primary regulating group R_2 within the regulation band range from 5.22×10^{-5} to 8.8×10^{-5} $\Delta\rho$/cm. The regulation band is located 140-180 cm from the reactor top. It can satisfy the requirements such as 10 percent step variation or 5 percent linear variation of the rated load, small distortion of axial power distribution, and small variation in critical boron concentration.

III. Fuel Management and Burnout Analysis

1. Fuel Management and Burnout Depth

The reactor operation of the nuclear heating and power plant consists of 37 life cycles of 37 reactor cores. At the end of one life cycle and the beginning of the next life cycle, the reactor is shut down, burned fuel is removed, and new fuel is loaded; thus, a new reactor core is formed to achieve the required

Table 2. Reactivity Distribution of Initial Reactor Core

Effects which cause loss of reactivity	Δ keff
Total residual reactivity of cold-state reactor core at the beginning of life	+0.277262
Temperature effect from cold-state to hot-state zero-power at the beginning of life	-0.051322
Doppler effect from hot-state zero-power to hot-state full-power at the beginning of life	-0.022969
Burnout effect during mid life of the initial cycle	-0.0954
Effect of solid burnable poison waste at the end of life	-0.012149
Equilibrium Xe effect at the end of life	-0.027092
Effect of poison of long half-life fission products at the end of life	-0.06833

Table 3. Control Calculations Under Different Conditions of the Initial Clean Reactor

Condition				k_{eff}
Operating condition	Burnable poison	Control rod	Boron concentration ppm	
Cold state	Yes	No	C	1.202143
Cold state	Yes	No	1098	1.0
Cold state	Yes	Yes	1098	0.9003
Cold state	Yes	Yes	352.22	1.0
Cold-state refueling	No	No	2200	0.90
Same as above	No	No	2650	0.85
Same as above	No	Yes	1500	0.90
Cold shut-down	Yes	No	1210	0.985
Same as above	Yes	Yes	451	0.985
Hot-state zero-power	Yes	No	1000	1.0
Same as above	Yes	Yes	0	0.983
Hot shut-down	Yes	No	1013	0.985
Same as above	Yes	Yes	0	0.964
Hot-state full-power	Yes	No	878.65	1.0
Hot-state full equilibrium X_e	Yes	No	636.61	1.0

Table 4. Composite Values of Control Rod Groups at the Beginning of Life and End of Life

Rod layout	Rod value Δρ%	
	Beginning of life	End of life
R_2	1,786	1.489
R_1	1.652	1.553
S_1	2.866	2.978
S_2	1.696	1.663
S_3	6.885	4.880
R_1+R_2	3.338	3.042
$R_1+R_2+S_1$	6.224	6.0197
$R_1+R_2+S_1+S_2$	7.920	7.683
$R_1+R_2+S_1+S_2+S_3$	14.805	12.564

residual reactivity, life cycle, coefficient of power non-uniformity, and burnout depth.

The fuel management of a reactor core consists of arranging the fuel boxes in a chess board pattern and pouring the fuel from outside toward the center. The initial fuel loading contains fuel modules with three different concentration levels: 2 percent, 2.4 percent and 3.1 percent which are distributed in 13, 16, and 16 boxes respectively. The refueling concentration level is 3.4 percent. Because the reactor has 45 boxes of fuel modules and is subject to the constraints of geometry and symmetry, it is difficult to achieve uniform and symmetric distribution of the fuel elements with 15 boxes each. But after 3 life cycles, periodic repetition of fuel management can be achieved.

We have explored many different forms of fuel management which can generally be divided into two categories: A and B. Category A is of the form 16-16-16; category B is of the form 12-16-16. In both cases the fuel modules at the center of the reactor core are not refueled; they contain only the 2 percent and 2.4 percent modules in order to avoid the sudden increase in the coefficient of power non-uniformity.

In category A, the 16 boxes are refueled uniformly, but one of the boxes is refueled only every two life cycles, thus the average burnout depth of the unloaded fuel is rather shallow. In category B, the refueling number of each reactor core is uneven, resulting in higher coefficient of power non-uniformity, but the average burnout depth of the unloaded fuel exceeds 30,000 trillion watt-day/ton (uranium), thus significantly improving the fuel economy.

2. Power Distribution and the Coefficient of Power Non-uniformity

The computations of fuel management, power distribution and coefficient of power non-uniformity are carried out using a two-dimensional coarse mesh program (with embedding) and a three-dimensional coars mesh program. Because of symmetry, only one fourth of the reactor core is included in the computation; the pattern used in the calculation is shown in Figure 2. Selected results of the coefficient of power non-uniformity are presented in Table 5, where k_{xy} denotes the coefficient of power non-uniformity averaged over the modules in the x-y plane; k_z is the axial coefficient of power non-uniformity of the corresponding hot box; k_p is the coefficient of power non-uniformity of the point embedded in the hot box; k_c denotes the circumferential coefficient of power non-uniformity of the fuel element; k_e denotes the engineering factor; and k_v is the total coefficient of power non-uniformity. The axial relative power distribution represents the average value of axial separation.

IV. Brief Description of the Computation Method

1. Calculation of Group Parameters

In the calculation of minor group parameters, the fast three group energy spectrum and group parameters are computed using the B_1 approximation fast group energy spectrum program; the thermal group energy spectrum and group parameters are computed using a thermal spectrum Monte-Carlo program. The

various reactivity temperature coefficients are computed using a special temperature calculation package. The parameters of the thermal spectrum are computed by a grid element subroutine based on first collision probability. The macroscopic absorption cross section of the control rod is computed using an ultra-thermal and thermal Monte-Carlo program.

Figure 2. Average Power Distribution in Two-Dimensional x-y Plane

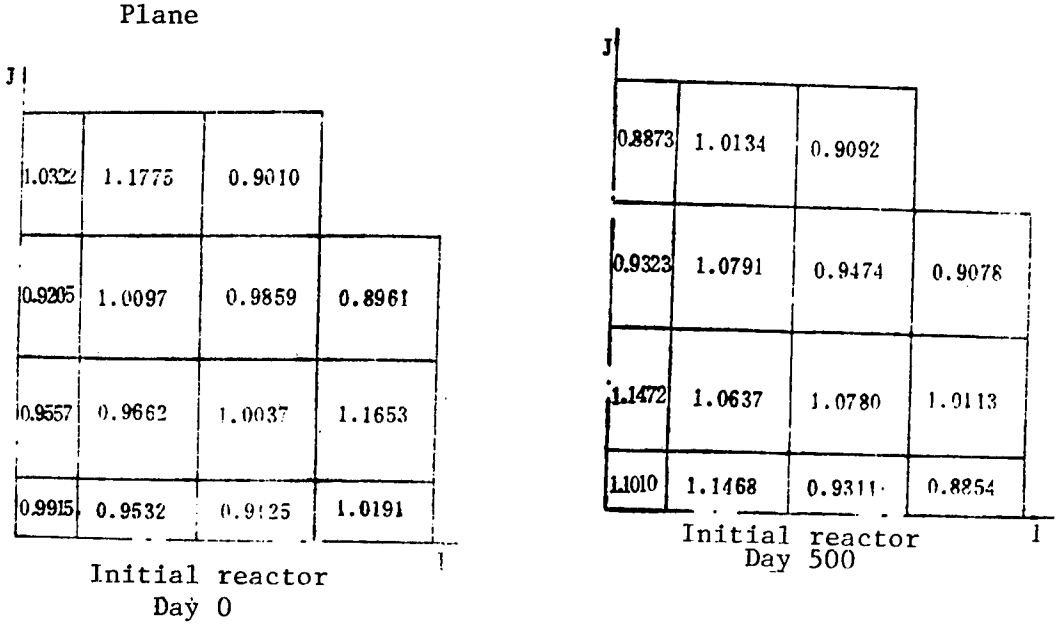

2. Critical and Burnout Calculations

The critical and burnout calculations of the reactor core are carried out using a minor group diffusion burnout program based on the two-dimensional (x,y) coarse mesh method and fine mesh method, and a fuel management program based on the three-dimensional (x,y,z) coarse mesh method.

The above computer programs can be used collectively as a package for the physical design of reactor core of a PWR. These programs have been tested using international benchmark problems; the computational methods and the reliability and usability of the programs have been verified. As a further verification, the programs have been used to calculate the performance parameters of a similar reactor core of a foreign country. The results show that the calculated error in k_{eff} was less than 1 percent, the calculated error in life cycle was around 3 percent and the calculated error in plutonium output was 2.4 percent.

Acknowledgement is due to comrades Liu Zhikun and Zhao Wei who also participated in the design work.

Table 5. Coefficient of Power Non-Uniformity and Axial Relative Power Distribution

Reactor Day	I-0	I-150	I-300	II-0	II-150	II-300	III-0	III-150	III-300
k_{xy}	1.1775	1.1933	1.1472	1.1560	1.1078	1.0920	1.2464	1.1612	1.0959
k_r	1.7350	1.3043	1.1773	1.2020	1.1023	1.1659	1.4030	1.0910	1.0635
k_z	1.1572	1.0485	1.0271	1.0200	1.0476	1.0470	1.0241	1.0594	1.0801
k_c	1.08	1.08	1.08	1.08	1.08	1.08	1.08	1.08	1.08
k_e	1.1	1.1	1.1	1.1	1.1	1.1	1.1	1.1	1.1
k_v	2.8086	1.9387	1.6480	1.6838	1.5198	1.5700	2.1275	1.5944	1.4955
Reactor hgt., cm	Axial relative power distribution								
273.0	0.11887	0.49663	0.66318	0.64743	0.67671	0.65006	0.35464	0.69861	0.84024
260.0	0.22194	0.83447	0.99659	1.06121	0.97012	0.82841	0.58155	0.99775	1.04900
246.5	0.37596	1.19981	1.27593	1.36549	1.16087	0.92593	0.77793	1.18775	1.15953
226.5	0.58598	1.46702	1.37063	1.48304	1.21852	0.92703	0.95040	1.25350	1.16312
206.5	0.83364	1.56098	1.32343	1.46127	1.20420	0.89759	1.11754	1.25337	1.13281
186.5	1.13483	1.53950	1.24347	1.40019	1.18033	0.89249	1.30643	1.24700	1.11215
166.5	1.47597	1.45964	1.19583	1.34429	1.16268	0.98154	1.52140	1.26618	1.12043
146.5	1.78317	1.36650	1.16533	1.29529	1.15448	1.05240	1.69875	1.27760	1.12872
126.5	1.96991	1.29033	1.15176	1.25159	1.15496	1.06328	1.79369	1.27114	1.12892
106.5	1.99549	1.24745	1.17278	1.22081	1.16443	1.07140	1.80826	1.26315	1.13455
86.5	1.86623	1.23011	1.22653	1.20270	1.18183	1.09341	1.75245	1.25928	1.15223
66.5	1.56480	1.19311	1.28006	1.17539	1.19205	1.12713	1.63383	1.24980	1.17919
46.5	1.14369	1.05011	1.23875	1.07294	1.13745	1.13396	1.42256	1.18594	1.17878
26.5	0.72831	0.78429	1.01775	0.84526	0.95662	1.03531	1.10049	1.00584	1.07521
13.0	0.40201	0.48697	0.70249	0.52458	0.67244	0.83164	0.68235	0.71223	0.86946
0.0									

3012/8918
CSO: 4008/76

12.5J KrF EXCIMER LASER PUMPED BY HIGH-INTENSITY RELATIVISTIC ELECTRON BEAM

Shanghai YINGYONG JIGUANG [APPLIED LASER] in Chinese Vol 6 No 2, Apr 86 pp 49-52

[Article by Wang Genchang [3769 3227 2490], Zhu Xuhui [6175 2485 6540], Wang Naiyan [3769 0035 1750], Xie Jinggang [6200 6955 0474], Li Yingshan [2621 7751 1472], Zhou Changzhun [0719 2490 0402], and Wang Pu [3769 3877] of the Institute of Atomic Energy, Chinese Academy of Sciences]

[Text] Abstract: A KrF excimer laser pumped by a high intensity relativistic electron beam at a gas pressure up to 3.5 atm. has been investigated. 12.5J laser energy was obtained at a total pressure of 3 atm for an Ar:Kr:F_2 = 89.6:10:0.4 mixture in an excitation volume of approximately 1.5 liters. The laser output energy was studied as a function of various parameters.

I. Introduction

Because of their great energy, high efficiency and short wavelength, electron beam pumped KrF excimer lasers are strong conditions for laser fusion and laser weapons. In the "Strategic Defense Initiative" plan, KrF lasers or beams amplified by free electron lasers will serve as the second line or third line interceptor weapons for missiles. Because of the short wavelength and the efficient energy coupling with the target sphere, KrF lasers can achieve a higher temperature.

The high current pulsed electron beam accelerator at the Institute of Atomic Energy in Beijing has been in operation since 1982 and performed reliably.[1] Recently we have developed a diode with a large area cathode and have extracted a large area electron beam to pump a KrF laser. We have also designed and built a laser pumped by a transverse electron beam. This laser had an output of 12.5J (almost 10J/1) when the cavity was filled with 3 atm of Ar, Kr, and F_2 in the ratio of 89.6:10:0.4.

II. Experimental Setup

The cathode of the large area diode is rectangular and measures 36 x 6 cm^2. It is made of brass and has a number of rectangular grooves. The anode is made of 50 μm thick aluminum foil. The electron beam is led out through a

40 x 8 cm^2 window. The electrodes are separated by a distance of 2-2.2 cm. The anode of the diode is grounded and the cathode is connected to the negative high voltage of a Marx generator through a water line. In the experiment the voltage of the diode is 0.5 MV, the peak current is 40 kA and the pulse width is 80 ns. The gas cell of the laser is 50 cm long, the activation zone is 40 cm long, the outlet aperture is 7 cm, and the total activated volume is 1.5 liters. The cavity is 60 cm long, one end is a 96 percent total reflection mirror, the other end is an output plane mirror with a variable transmissivity of 40 to 70 percent. The end connected to the accelerator has a 38 x 8 cm^2 frame with stainless steel support rod for the 25 μ titanium film and separating the gas cell from the vacuum chamber of the accelerator. The experimental setup is shown in Figure 1.

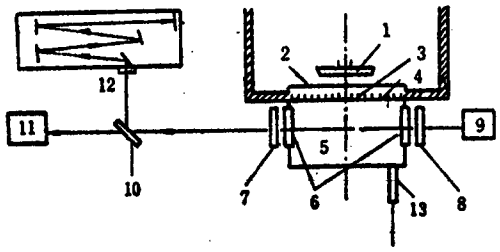

Figure 1

To test the laser parameters, a large aperture model JN-1-A energy meter is installed at the output of the laser. The pulse width of the laser and the pluorescence is measured at the other end using a model GD-51 photoelectric cell. The spectral lines are recorded by a model WSP-1 2 meter grating spectrophotometer and analyzed by a 3 CS microdensitometer. The divergence angle of the laser is photographed and computed with a focal spot method. The homogeneity of the laser is recorded with an acid sensitive metachromatic plate, and analyzed with a scanning microdensitometer.

III. Experimental Results

1. Parameters of the KrF laser

For a gas mixture ratio of $Ar:Kr:F_2$ = 89.6:10:0.4 and a total gas pressure of 3 atom, the maximum output energy of the KrF laser is measured to be 12.5J, or approximately 10 J/liter. The overall efficiency is about 1 percent.

The voltage waveform of the diode is measured with a high voltage oscilloscope. The current waveform is measured with a Faraday cylinder (see Figures 2 and 3). The accelerator parameters are 0.5 MW, 40 kA, and 80 ns. The laser and fluorescence waveforms are measures with a GD-51 photodiode and the widths are respectively 70 ns and 100 ns (Figures 4 and 5).

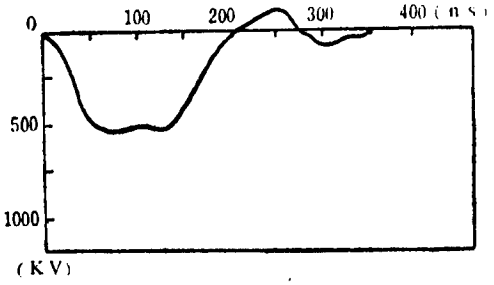

Figure 2

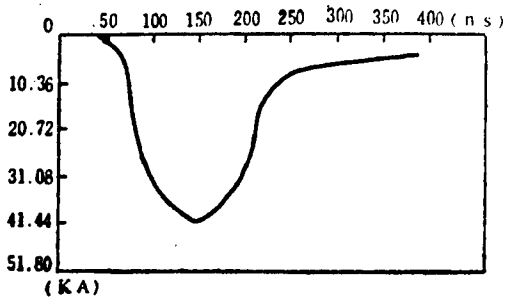

Figure 3

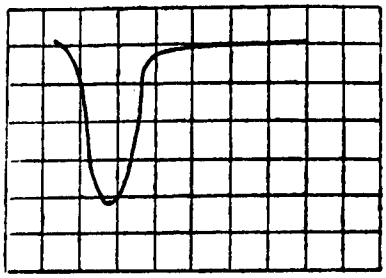

Figure 4

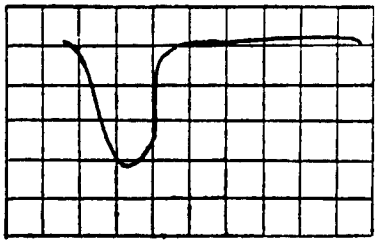

Figure 5

The laser and fluorescence spectral lines of the KrF laser are photographed with a 2-meter grating spectrophotometer. In filming the laser spectral lines, an attenuation of 500 or greater is used. Multiple exposure is used in filming the fluorescence for clear display. The photographic plates are analyzed with a microdensitometer. Figures 6 and 7 show the intensity distribution of the laser and fluorescence spectral lines. The widths at half maximum are respectively 5 A and 30 A for the laser and fluorescence spectral lines.

The divergence angle of the parallel plane cavity is measured using the focal spot method. The divergence angle is found to be 10 mrad, apparently too large. The large divergence is attributed to two causes: first the quality of the cavity mirror is poor and the mirror is convex instead of planar; second, the normal of the two quartz window plates is not separated from the laser axis. Researchers abroad generally use a 15 degree tilt; but, due to difficulties in fabrication, we did not tilt the quartz windows. As a result, the quartz windows form a subsidiary resonance cavity with the laser cavity mirror (especially the reflection mirror) and the focal spot becomes elliptical and the divergence angle becomes large. The beam quality will be improved in the future by using an unstable cavity.

The uniformity of a laser is determined mainly by the uniformity of electron beam pumping of the gas. Since we used transverse pumping by a single electron beam, the electron density decreases along the beam propagation direction, causing the laser intensity to decrease. An acid sensitive

metachromatic plate that changes color under ultraviolet light is directly exposed by the laser. The plate is then scanned by a microdensitometer and the result is shown in Figure 8.

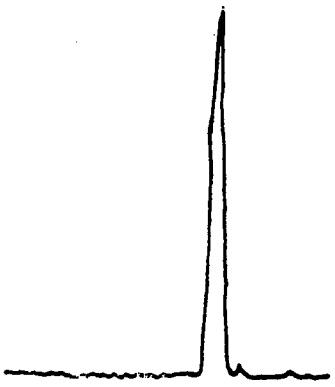

Figure 6

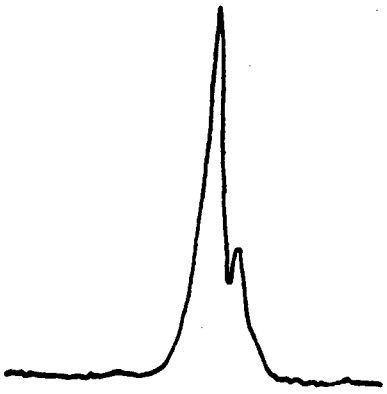

Figure 7

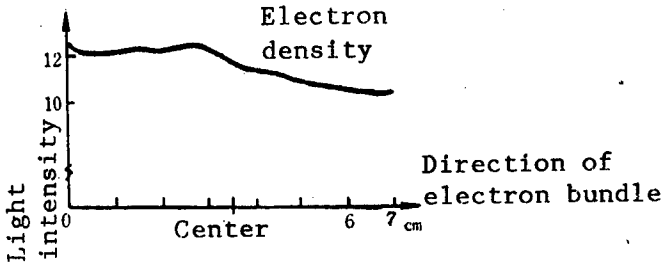

Figure 8

2. Effects on the laser output

Work in this area has not been completed and the results are preliminary.

We measured the effect of the gas pressure on the output energy of the laser. While keeping the mixture ratio at $Ar:Kr:F_2$ = 89.6:10:0.4, the total gas pressure was changed from 1.5 atm to 3.5 atm and the laser output energy was measured by maintaining the same discharge condition. Figure 9 shows that, within our experimental range, the output laser energy depends first linearly on the total gas pressure but the rate of increase drops when the gas pressure further increases. Evidently, at the large electron beam energy (0.5 MeV), an increase in gas pressure increases the energy deposition and the corresponding laser output.

We investigated the relationship between the laser output energy and the transmissivity of the output mirror. The reflectivity of the total reflection mirror was held constant at 96 percent and the output energy was measured for

four different output mirror transmissivity: 40, 55, and 70 percent. Figure 10 shows that the range studied was not wide enough to locate the optimum value. It can be seen, however, since the gain of a KrF laser is very high, the transmissivity of the output mirror can still be made higher. In fact, it was observed experimentally that, even without an output mirror, the quartz window and the total reflection mirror can form a resonance cavity and produce a laser output.

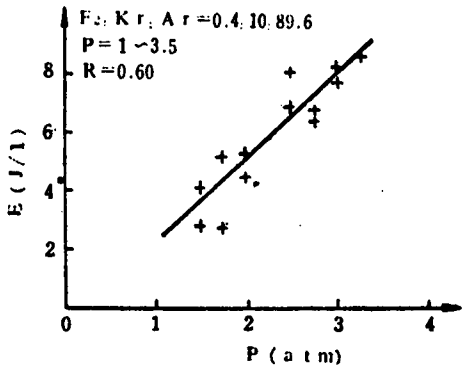

Figure 9

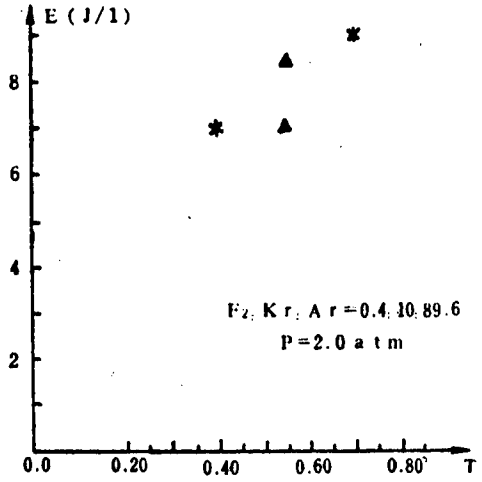

Figure 10

IV. Theoretical Calculation

The Monte Carlo method was used to calculate the trajectory and the energy loss of an electron in the gas. The ETRAN program[2] was simplified for the specific calculation of an electron beam pumped excimer laser. Only the deflection angle and ionization energy loss were computed. A CYBER-825 computer was used to compute a particle ensemble of 100. Figure 11 shows the dynamic process of electron excitation in a 2 atm argon gas atmosphere in a KrF laser. The average energy loss of the electron was computed to be 65 keV for a propagation distance of 7 cm.

Table 1 shows that the characteristics efficiency of the laser is about 10 percent. The electron energy deposition power is also about 10 percent and the total efficiency is about 1 percent.

Using the rate equation, simulation calculations were made for the electron beam pumped KrF laser. Using a nonsteady state equation and the current pulse waveform of the electron beam, the temporal waveforms of the KrF laser and fluorescence, the time dependent particle densities, and the output laser energy were computed. The calculated and experimental results showed that the temporal waveforms of the laser pulse was very similar to that of the electron beam current. One can therefore simplify the problem by using the steady state equation as an approximation. On this basis the laser efficiency was

computed as a function of the excitation rate and the output energy was computed as a function of the output mirror transmissivity. Finally we obtained the principal channels and their percentages for the KrF excimer generation under our experimental conditions. In the future we shall further improve the laser efficiency, improve the beam quality and generate other excimer lasers.

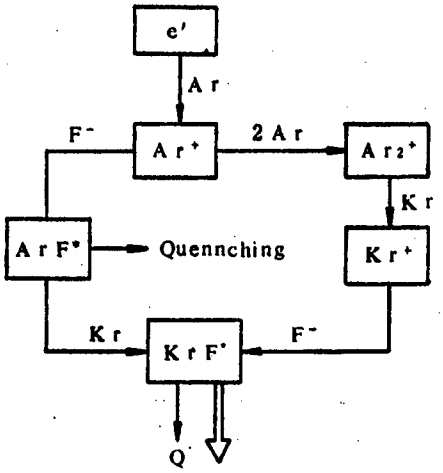

Figure 11

Table 1. Relationship Between the Electron-Energy and the Laser Energy

Diode tube	0.5 MeV	40 KA	80 ns	1,600 J
Cavity input	0.46 MeV	30 KA	60 ns	900 J
Calculated energy deposition	65 Kev	30 KA	60 ns	120 J
Measured laser energy			70 ns	12.5 J

REFERENCES

1. Wang Ganchang, et al., HEKEXUE YU GONGCHENG [NUCLEAR SCIENCE AND ENGINEERING], 1985, No 1, p 1.

2. M. J. Berger and S. M. Seltzer, National Bureau of Standards Report, No 9836 (1986).

9698/9599
CSO: 4008/67

APPLICATION OF He-Ne LASER HOLOGRAPHY IN SUPERSONIC WIND TUNNEL FLOW FIELD

Shanghai YINGYONG JIGUANG [APPLIED LASER] in Chinese Vol 6 No 2, Apr 86 pp 63-68

[Article by He Xiulin [6320 4423 3829], Xu Zhaoshun [1776 0340 7312], Dai Siping [2071 1835 1627], Zhang Jingdong [1728 2417 2639], and Ye Yanje [0673 1693 3381] of the A. I. M. No 633 Research Institute]

[Text] Abstract: This paper discusses the applications of He-Ne laser holography in the quantitative visualization of the supersonic wind tunnel flow fields. Computation results of two axially symmetric flow fields are given. The experiments show that holographic interferometers based on a He-Ne laser can be applied to not only small wind tunnels but also large wind tunnels.

I. Introduction

Optical measurements play an important tole in flow field display. As compared to classical optical measurements, laser holography not only is accurate, tunable and costs less, but also contains a wealth of information and affords quantitative computation. Almost all wind tunnel flow display systems based on laser holography employ pulsed ruby laser (or high repetition rate YAG laser) as the recording light source and He-Ne laser as the reconstruction light source. Tanner[1] has used a He-Ne laser in wind tunnel experiments but his recording and reconstruction setups were complicated and required stringent optical tolerance and the system can only be used in small wind tunnels. The experimental results on the field flow of supersonic wind tunnels presented in this paper are obtained with a system that uses He-Ne lasers as the recording and reconstruction sources. Because He-Ne lasers are more stable than ruby lasers, easier to operate, and less costly, they are more desirable in actual applications.

II. Principles

The flow field of a wind tunnel is a variable density field. The refractive index n is a function of the media density. When light passes through a flow field, the optical paths are different at different parts of the field. The optical path is defined as $\Phi = n \cdot L$ where L is the lateral distance of the

experimental section of the wind tunnel, and the corresponding phase shift is $\delta = 2\pi\Phi/\lambda_0$.

If the density field around the model can be measured, then considerable flow field information may be extracted from the data. Using laser holography, one may record and reconstruct the density of the flow field and the changer of the density for a change in time Δt. The light intensity distribution[2] of a double exposure holograhic reconstruction is

$$I \propto \cos^2\left[\frac{1}{2}(\delta_{01} - \delta_{02} + \Delta)\right]$$

where $(\delta_{01} - \delta_{02})$ is the phase difference of the object light between the two exposures, Δ is a reference light phase change introduced for the sake of computation. The signal on a given point on the recording plane is the sum of the density changes at all points in the flow field sensed by the light. If the objective light beam is along z axis, then the interference fringe distribution function is

$$S(x.y) = \frac{K}{\lambda}\int_{z_1}^{z_2}[\rho(x.y.z) - \rho_0]dz$$

where K is the Dale-Gladstone coefficient and ρ_0 is the density in absence of the flow field. For a two-dimensional wedge,

$$S = KL(\rho - \rho_0)/\lambda$$

For an axially symmetric flow and in the x = constant cross-section, we let

$$z^2 = r^2 - y^2$$

After a coordinate transformation, we obtain the Abel equation,

$$S(y) = \frac{K}{\lambda}\int_0^{\sqrt{R^2-y^2}}[\rho(r) - \rho_0]\frac{d(r^2)}{\sqrt{(r^2 - y^2)}}$$

The chosen cross-section is then divided into N concentric rings with equal width (W). The radii r_i are:

$$0 = r_0 < r_1 \cdots < r_i \cdots < r_\mu \cdots < r_N = R,$$
$$r_i = iw, \quad r_\mu = \mu w_o$$

We also let $\nu_i = [\rho(r_i) - \rho_0]K$. Based on different assumptions we have the following approximate solutions:

1. Linear function method[3]

$$\nu_i = \left[\frac{\lambda}{W} S(r_i) - \sum_{\mu=i+1}^{N-1} \nu_\mu B(i, \mu)\right] / A(i)$$

$$A(i) = 2\sqrt{2i+1}, \quad B(i, \mu) = A(i, \mu) - A(i, \mu-1)$$

$$A(i, \mu) = (\mu+1)\sqrt{(\mu+1)^2 - i^2} - \mu\sqrt{\mu^2 - i^2} - i^2 \ln \frac{(\mu+1) + \sqrt{(\mu+1)^2 - i^2}}{\mu + \sqrt{\mu^2 - i^2}}$$

$$(i = 0, 1, 2 \cdots N-1)$$

2. Step function method

$$\nu_i = \left[\frac{\lambda}{2W} S(r_i) - \sum_{\mu=i+1}^{N-1} \nu_\mu B(i, \mu)\right] / B(i, i)$$

$$B(i, \mu) = \sqrt{(\mu+1)^2 - i^2} - \sqrt{\mu^2 - i^2}$$

3. Quadratic function method

$$\nu_i = \frac{2\lambda}{\pi W} \sum_{\mu=i}^{N-1} \frac{(S_\mu - S_{\mu+1})[\sqrt{(\mu+1)^2 - i^2} - \sqrt{\mu^2 - i^2}]}{2\mu+1}$$

4. Power series method[4]

$$S(t) = \sqrt{t} \sum_{n=0}^{\infty} B_n t^n$$

where B_n are coefficients to be determined from a least squares fit to the power series ($n = 3$ in our experiment) and $t = 1 - (y/R)^2$.

When the flow field is conical, the values of $(\rho - \rho_\infty)$ for a given polar angle is a constant and independent of the cross-section on which readings are taken. For the convenience of computation, we set the fringe drift number $S_0 = \frac{\rho_\infty - \rho_0}{\lambda} KL \equiv 0$, ρ_∞ to zero at the intersection of the cross-section chosen and the shock wave surface. Here ρ_∞ is the beam density of a constant current.

The density jump caused by the sudden compression of the air near a shock wave is given by

$$\rho - \rho_\infty = \rho_\infty \left[\frac{(\kappa+1)/(\kappa-1)}{1 + 2/(\kappa-1)M^2 \sin\beta} - 1\right]$$

In our experiment $\kappa = C_p/C_v = 1.4$. The value of ρ_∞ is determined from the equation of state

$$P_0/\rho_0 = RT_0$$

and the isentropic relationship

$$p_0/\rho_\infty = \left(1 + \frac{\kappa - 1}{2} M^2\right)^{1/\kappa - 1}$$

By measuring the fringe drift number, the corresponding density can be computed.

III. Experimental Setup

The experiments were conducted in the instructional wind tunnel at the Applied Mathematics Department of Fudan University and the NH-1 wind tunnel of the Nanjing Aeronautical College.

1. The Fudan wind tunnel is a transient pulse type wind tunnel. The experimental section has an equarional structure. The observation window is a 10 mm thick glass plate with an aperture of 80 mm diameter. The noise level of the vibration is 120 dB. The experimental setup in placed on both sides of the antivibration platform of the tunnel. The platform consists of two 18 mm thick steel plates held together securely by three pieces of channel steel passing under the experimental section. An inner tube of an automobile tire is placed under each of the plates. The experimental models are a two-dimensional wedge (Figure 1) and a steel cone with a half angle of 15 degrees (Figure 2). The Mach numbers are respectively 2.3 and 2.23.

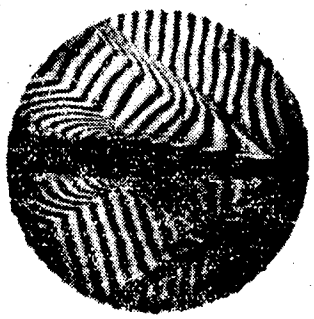

Figure 1. Holographic Interference Pattern of the Wedge at Mach 2.3

Figure 2. Holographic Interference Pattern of the Cone at Mach 2.23

2. The NH-1 wind tunnel at the Nanjing Aeronautical College is a direct current, transient pulse, down blow type wind tunnel with a nominal wind speed of Mach 3. It has two element rigid wall nozzles. The experimental section measures 600 x 600 mm and can accommodate almost all experiments normally performed in a large scale high sonic speed tunnel. Both sides of the observation window have two layers of optical glass. The vibration noise is 160 dB.

The experimental setups are placed on the two independent platforms on the two sides of the tunnel. The platform faces are the nozzle walls. The frame is constructed out of 3 cm steel tubing, and 3 mm thick 3 cm wide angle irons. The frame is separated from the ground only by a 4.5 cm thick foamed plastic insulation. On such a crudely constructed platform, we have obtained good holograms (Figures 3 and 4) on a conical model with a half angle of 15 degrees at Mach 2.0.

Figure 3. Finite Fringe Holographic Interference Pattern (M = 2.0)

Figure 4. Infinite Fringe Holographic Interference Pattern (M = 2.0)

The recording and reconstruction source is a 1 meter long He-Ne laser with a single transverse mode and 10 longitudinal modes. The output power is 30 mW, the wavelength is 9328 A, the recording medium is a Tianjin I holographic plate and the exposure time is 1/1000 second.

IV. The Optical Path

We used a double exposure method and recorded two holograms on the same plate. The two exposures were made with the tunnel empty and with the wind going. Figure 5 shows the optical path. The reference beam may go around the

outside the tunnel (Figures 1 and 2) or go through the unperturbed region of the flow field in the experimental section (Figures 3 and 4). Clear interference figures were obtained in both cases.

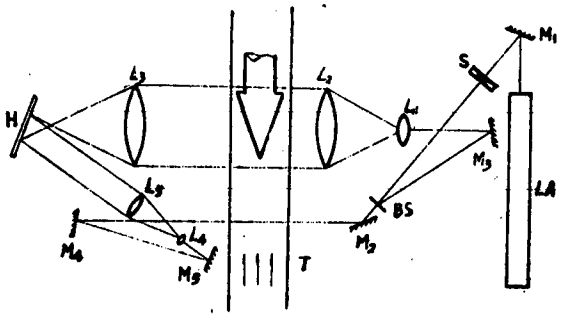

LA	Laser
M	Reflection mirror
BS	Beam splitter
H	Holographic plate
S	Shutter
L	Lens
T	Tunnel

Figure 5. Experimental Optical Path

When the holographic interferometer is used on a large wind tunnel, the exposure cannot reach the linear region on the t-E curve because of the low output power of the He-Ne laser and the slow speed of the Tianjin I_2 holographic plate. The optimum exposure of this plate is 30 mJ/cm^2 and the exposure time must be less than 1/1000 second. To increase the light energy density, we focused the recording beam on the plate to reach the optimum exposure energy density. This has circumvented the difficulties of the low laser power, the high flow field speed and the vibration of the model.

V. Results, Analysis, and Discussion

We shall present the calculated results only for two conical flows. The fringe counting was made with a measuring microscope and the data processing was done on a PDP11/23 microcomputer. The theoretical values were taken from Reference 5.

The flow field shown in Figure 1 is not a simple symmetric field. Because of the finite distance between the wedge and the observation window, the problem cannot be reduced to a two-dimensional one. In addition to two shock waves associated with the object, there are five additional discernable wave traces. They are produced mostly by the step on the tunnel wall that has not been taken into account in the reconstruction computation.

Figure 6 shows the comparison of the calculated results of Figure 2 and the theoretical value. The errors are greater at the mid-section of the curve. For the cross-section in Figure 2 (about two-thirds from the apex), an external shock wave passed through. This shock wave was caused by the step in the tunnel wall. It directly affected the density in the conical flow and led to further compression.

Near the tail of the model, an inflection point appeared in the interference fringes. Within the fan sector between the inflection point and the frame rod, the flow decreased suddenly and the speed increased. This region is

usually referred to as the expansion zone. Laser holography provided us a direct way to visualize and analyze the expansion zone. In fact, the density field of the expansion zone has axial symmetry and satisfies the Abel equation. Using the above method, it is not difficult to obtain a quantitative solution, but eddies at the location where the frame rod is normal to the cone complicate the flow field.

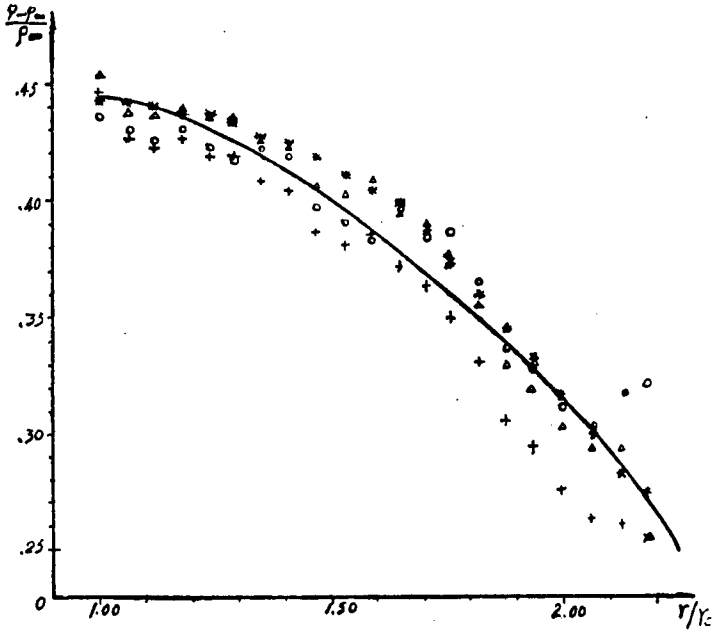

Figure 6. Comparison With Theoretical Values

*	Power series method	Δ	Step function method
x	Linear function method	o	Quadratic function method

Solid line represents the theoretical values and r_c is the radius of the cone at the chosen cross-section

Figure 3 shows the axially symmetric flow field of the NH-1 wind tunnel for a zone attack angle and at M = 0. The interference fringes are clear and the calculated results (Figure 7) agree with the theoretical values. This has demonstrated that He-Ne lasers are applicable not only on small wind tunnels but also on large wind tunnels as a holographic recording light source in flow field display.

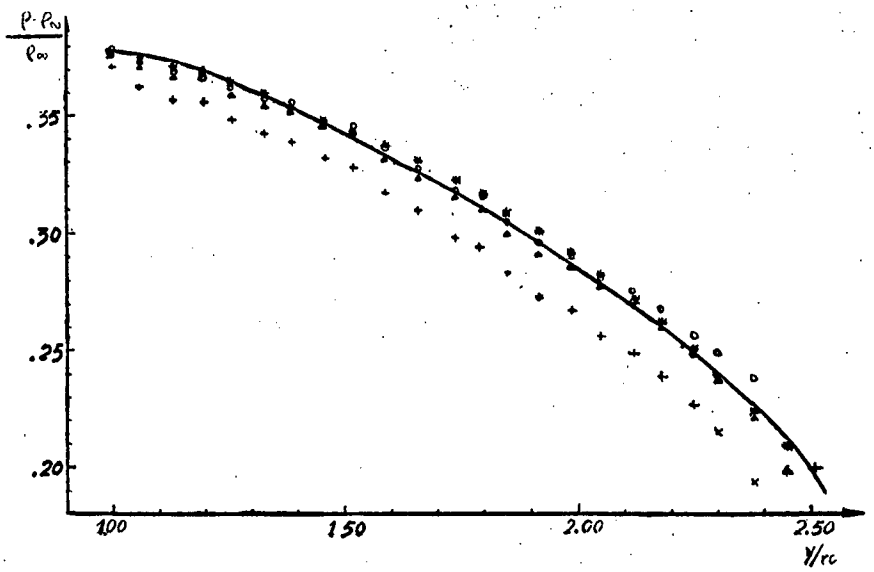

Figure 7. Comparison With the Theoretical Values
(Legends see Figure 6)

Figure 4 shows the infinite interference fringe hologram for the NH-1 tunnel. It clearly shows that the antivibration setup used in this experiment is safe and meets the requirements. For an exposure time less than 1/1000 second, antivibration measures are not needed. Existing fringe photographic equipment (all units with a wind tunnel are equipped with such equipment) are adequate in filming the flow field. Although the hologram contains the shadow signal and the fringe signal, the laser shadowgram and the fringe pattern may be obtained readily and directly, as shown in Figures 8 and 9. The information content is obviously greater than the usual shadowgram and fringe pattern. He-Ne lasers therefore possess great application values in the flow field visualization for wind tunnels.

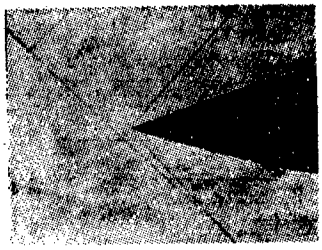

Figure 8

Figure 9

The experiment may benefit from the following improvements:

1. The photos showed diffraction fringes around the model. To obtain a clear boundary, the objective light beam may be passed through a diffusely scattering ground glass plate before passing through the flow field. This

would not only improve the image quality but also make the hologram contain three-dimensional information.

2. The photo in Figure 3 has speckle noise, which causes problems in image analysis by the computer. The speckles are determined by the image formation characteristics and the aperture. One way to solve such problem is to place the recording medium in the vicinity of the back focal plane of the image forming lens (moving toward the lens) to form a near Fourier transform holograph. This would greatly suppress the effects of speckle without degrading the diffraction efficiency excessively.

Since the light energy density on the recording medium was increased considerably, the exposure time is greatly reduced to 10^{-5} sec. The effect is even better with a high speed film. With such short an exposure time, the He-Ne laser holography technique cannot only display a steady flow field, but also record transient changes of some flow fields.

The authors gratefully acknowledge the help lent by Professors Xu Youheng [1776 2589 1854] and Mu Sheng [4476 8508] of Fudan University and Professors Wang Qiaosen [3076 0829 2773] and Chang Renquan [4453 0088 0356] of the Nanjing Aeronautical College.

REFERENCES

1. L. H. Tanner, Opt. & Laser Tech., 4, No 6, 281 (1972).

2. He Xiulin, et al., Measurements and Microcomputers, 1985, No 2, p 33.

3. R. W. Laden, Princeton Series on High Speed Aerodynamics and Jet Propulsion, 1954.

4. J. Bradley, AIAA J. 6, 1190 (1968).

5. Table Supersonic Flow Around Cones, Vol 1, 1947, and AD-698779 AGAR Dograph 137.

9698/9599
CSO: 4008/67

ATOMIC-VAPOR LASER URANIUM ISOTOPE SEPARATION

Shanghai YINGYONG JIGUANG [APPLIED LASER] in Chinese Vol 6, No 3, Jun 86 pp 131-134

[Article by Lin Fucheng [2651 4395 2052] of the Shanghai Institute of Optics and Fine Mechanics, Chinese Academy of Sciences]

[Text] Abstract: The essential concepts and recent advances of atomic-vapor laser uranium isotope separation are reviewed in this paper.

I. Introduction

China is rich in energy resources. It has verified coal reserves of 622.4 billion tons, 360 million kilowatts of water resources that may be developed, considerable reserves of oil and gas, and a reserve of natural uranium that can supply 15 million kilowatts of nuclear power plants for 30 years. However, China is also currently very backward in energy utilization. In 1980 the Chinese per capita energy consumption was only about one-fourth that of the world average. Large areas in China are under a shortage of energy supply, seriously affecting industrial and agricultural production and the standard of living. To accomplish the four modernizations, the estimated per capita energy consumption in the year 2000 will be about four times the current level.[1]

The types of energy and their geographic distribution are very lopsided. Shanxi and Nei Monggol have 61 percent of all the coal reserves in China, and the southwest region has 70 percent of all the water resources. The eight southeastern provinces and one municipality, with 40 percent of the population and 40 percent of the industrial and agriculture value of production, heavily depend on energy from elsewhere. Other regions such as Liaoning, Shandong, Anhui, Henan and Sichuan will soon have energy shortages. The above energy deficient regions have 77 percent of the total population and 80 percent of the industrial and agricultural value of production. An overall energy policy for China must seriously consider the utilization of nuclear energy. The advantage of nuclear energy is that it is essentially free from the fuel transportation problems and it may supply the southeastern coastal provinces and cities with energy. In addition, based on the coal price on the international market, the costs for nuclear energy in most of the regions in China will be

less than that of thermal power and the surplus coal and petroleum may be exported for economic gain. It is estimated that by the year 2000 the world will have 10,000 tons of separation power nuclear fuel per year, at a cost of 1 billion U.S. dollars. If the cost of Chinese-produced nuclear fuel is less than $60/kg in separation power, China may then compete in the world market.

II. Nuclear Fuel and Separation Process

Today the most common type of nuclear power reactor in the world is the pressurized water reactor (PWR). In the PWR, ordinary water (light water) is used as the moderating and reflecting material and for carrying the heat generated in the nuclear fission to the heat exchanger, as shown in Figure 1. The pressure of the water is maintained up to 160 atm by a pressurizer so the boiling temperature is above 300°C.

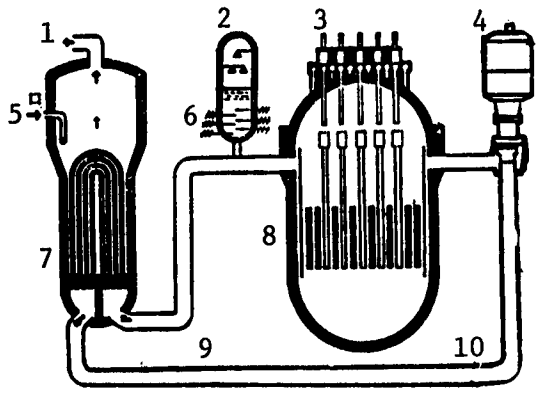

Key:
1. Steam line
2. Pressurizer
3. Control rod
4. Coolant pump
5. Feed water
6. Heating rods
7. Steam generator
8. Fuel
9. Pressurized line
10. Reactor pressure vessel

Fig. 1. Pressurized water reactor

In a PWR the nuclear fuel must contain 3.2 percent of ^{235}U. Since the ^{235}U content of natural uranium is only about 0.711 percent, natural uranium must be enriched or separated. The ratio of $^{235}U/^{238}U$ in the product and $^{235}U/^{238}U$ in the raw material fuel is known as the enrichment coefficient β_1 of the separation process:

$$\beta_1 = \frac{^{235}U/^{238}U \text{ (separation product)}}{^{235}U/^{238}U \text{ (fuel)}} \qquad (1)$$

The value of β_1 for a PWR is therefore 4.6. In any separation process, "tailings" with a depleted ^{235}U content are produced. The depletion coefficient β_2 is defined as

$$\beta_2 = \frac{^{235}U/^{238}U \text{ (fuel)}}{^{235}U/^{238}U \text{ (tailing)}} \qquad (2)$$

In order to make full use of the uranium material, the greater the β_2 the better. In current processes, the ^{235}U content in tailings is about 0.2 percent, that is, β_2 is about 3.6.

To quantify the work in a separation process, a "separation work unit" (SWU) is introduced. From the thermodynamics, the entropy is decreased and the free energy is increased when two isotopes are separated from a mixture. Let the ^{235}U contents in the fuel, the product, and the tailing be respectively X_F. X_P, X_T, one may define a SWU, in units of kilograms, directly proportional to the increase of the free energy in the separation process. The expression is

$$\frac{\text{SWU(kg)}}{\text{fuel(kg)}} = \left(\frac{X_T - X_F}{X_T - X_P}\right)V(X_P) + \left(\frac{X_F - X_P}{X_T - X_P}\right)V(X_T) - V(X_F) \tag{3}$$

where

$$V(X) = (2X - 1)\ln\left(\frac{X}{1 - X}\right) \tag{4}$$

Figure 2 is a graphical representation of Equation (3).

As can be seen, SWU/fuel depends strongly on the depletion of the tailing (X_T). The smaller the X_T, the greater the SWU/fuel. It depends very weakly on X_P and is essentially independent of X_P for X_P greater than 5 percent. As a special case, when there is no depletion of the tailing (X_T = 0.711 percent), the SWU per kilogram of fuel is zero. In the "standard" separation process, X_P = 3.2 percent, X_T = 0.2 percent, and SWU is 0.8 kg for every kilogram of fuel processed. Under these conditions, the product is 0.17 kg and the tailing is 0.83 kg. Table 1 shows the conversion relationships for the standard conditions.

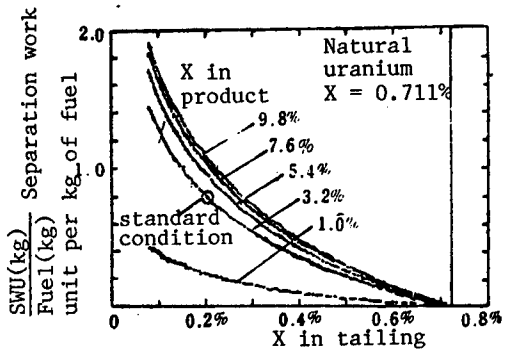

Fig. 2. X_T, X_P relationship in Eq. (3)

Table 1. Conversion under standard conditions

	SWU	Fuel	Product	Tailing
SWU	1	1.24	0.21	1.03
Fuel	0.81	1	0.17	0.83
Product	4.74	5.88	1	4.88
Tailing	0.97	1.20	0.20	1

Today the annual world consumption of nuclear fuel is about 25×10^8 SWU and the price per each kilogram of SWU is about $100. Each 10^3 SWU of nuclear fuel may supply a 10^4 kilowatt of nuclear power station for a period of one year.

III. Major Separation Methods and Activities Abroad

(1) Diffusion Method--By passing a pressurized UF_6 gas through a porous membrane, ^{235}U and ^{238}U may be separated since their diffusion rates are different. The β_1 for stage is about 1.004 and 1000 diffusions are needed. For economic reasons, the compressor must be very large and the building costs for a dissusion plant is therefore very high. Moreover, this separation method is very inefficient since the separation of each ^{235}U atom requires 3MeV of energy.

(2) Centrifuge Method--In a high speed centrifuge, the different masses of ^{235}UF and ^{238}UF in UF_6 give rise to a spatial distribution separation. The value of β_1 in this method is about 1.1, much greater than that of the diffusion method, and the energy required for separating a ^{235}U is also much less. Since the rotational speed of the centrifuge is very great, the centrifugal force experience by the centrifuge itself may exceed the material strength limit when the diameter is large. The size of each centrifuge is therefore limited and so is the production rate.

(3) Laser Method--The laser method may be divided into the molecular method and the atomic method. The molecular method makes use of the minute difference of the vibrational-rotational spectra of $^{235}UF_6$ and $^{238}UF_6$ and, by selective excitation of $^{235}UF_6$, $^{235}UF_5$ is collected after multiphoton dissociation. The atomic method makes use of the small spectral difference of ^{235}U and ^{238}U in atomic uranium vapor and, by selectively ionizing ^{235}U, collects the $^{235}U^-$ ions.

In the United States uranium has been produced mostly by the diffusion method. In West Germany and in the U.K., the centrifuge method is the main method. On 30 April 1982 the U.S. Department of Energy announced that, among the three

new methods for uranium separation--the laser atomic method, the laser molecular method, and the plasma method, the atomic method has been chosen to receive U.S. DOE support. On 15 May 1985 a technical evaluation committee of the U.S. DOE evaluated two advanced uranium enrichment methods, the gas centrifuge method and the laser atomic method, and announced on 5 June that the U.S. DOE will (1) shut down the Oak Ridge uranium diffusion plant, (2) halt the construction of the uranium centrifuge plant at Portmuth, and (3) adopt the laser atomic method as the uranium enrichment production technology for the next century and discontinue the effort on the advanced gas centrifuge method. After severe competition, the laser atomic method has finally established its status as the optimum technology for uranium enrichment.

France, with the most advanced uranium enrichment technology in western Europe, has been concentrating on the laser atomic method as the next generation technology and plans to start building laser enrichment plants in 1995. Japan has always directed its attention to the centrifuge method and has repeatedly announced that its principal technology is the centrifuge method. Under the impact of the U.S. decisions, Japan has also announced that it would give the centrifuge method and the laser method the same attention.

IV. Laser Atomic Method for Uranium Isotope Separation

The ionization potential of an uranium atom is 6 eV and several hundred energy levels have been identified for an uranium atom. Using a modern high resolution spectrometer, a total of 3×10^{-5} spectral lines have been observed in UI and UII. The spectral density in the 18,000-34,500 cm^{-1} range is 25 lines per Angstrom. Such high spectral density naturally makes spectral analysis very difficult, but it also provides ample choices in the laser atomic separation of uranium. The isotope shift of ^{235}U and ^{238}U is mainly a volume effect and the magnitude is about a few GHz. ^{238}U has a spin I = 0 and has no hyperfine structures. ^{235}U has a spin of I = 7/2 and 8 strong hyperfine structural lines covering a total width of a few GHz. For a uranium vapor temperature of $T \geq 2600$ K, the Doppler width is of the order of 1 GHz. The hyperfine structures of ^{235}U therefore cannot be clearly separated. Using the laser atomic method, a spectral line is selected and the isotope shift of ^{235}U relative to ^{238}U must be made greater than the hyperfine structure width of ^{235}U itself so that ^{238}U will not be excited when ^{235}U is excited. The spectral selectivity S is defined as the ratio of the absorption cross-sections of ^{235}U and ^{238}U at the center of a ^{235}U spectral line. S is usually greater than 10^4 and the chances for exciting a ^{238}U by mistakes is therefore very small. In this regard the laser atomic method is superior to the laser molecular method.

Since there is no laser with a fixed wavelength that exactly matches the ^{235}U excitation, a tunable dye laser must be used. With the broad selection of wavelengths, a high efficiency dye laser such as that uses Rhodamin 6G with a wavelength of 600 nm may be used. A three step excitation is needed to

reach the 6 eV ionization potential. Based on the measurement of energy level transitions of U atom, the absorption cross-section for light σ is about $10^{-14} \sim 10^{-17}$ cm^2 and the lifetime of the energy level τ is about 10^{-7} seconds. For the excitation rate $Nn\sigma$ to be greater than the deexcitation rate N/τ, the laser power density P must be greater than 1 kW/cm^2, see Figure 3. From the discussion below, the area of the light beam should not be too small, 10 cm^2 or so is needed. The power of the tunable dye laser is therefore greater than 10 kW. This rules out CW dye lasers and a pulsed laser must be used. The pulse width should be comparable to τ or 10^{-7} sec.

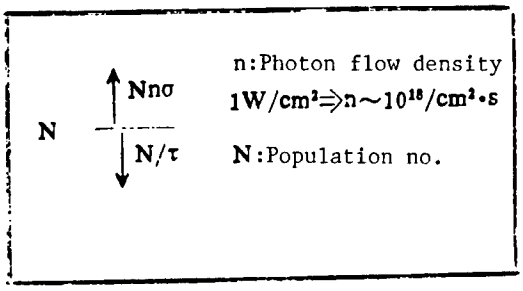

Fig. 3. Competition between excitation and deexcitation

At 2600°K, the velocity of the atomic beam is about 4×10^4 cm/s. For a beam diameter of 4 cm, it takes about 10^{-4} sec for new atoms to replenish the positions of ionized atoms after one excitation-ionization cycle. The laser needs to send out the second pulse after 10^{-4} sec and the repetition rate is therefore 10 kHz. Today there is only one laser capable of pumping a dye laser at this high repetition rate and that is the copper vapor laser with an output wavelength of 510.6 nm and 578.6 nm, a repetition rate of a few kHz and an efficiency of 10^{-2}. With the high efficiency Cu-dye laser system, the atomic method becomes even more superior to the molecular method. The molecular method calls for a 10μ laser and the efficiency is much lower. The average power (P(W) of a laser may be expressed by the following formula[2]:

$$\overline{P}(W) = 5.67 \times 10^4 \frac{M(SWU/year)h\nu(MJ)}{\eta} \qquad (5)$$

where η is the photon utilization rate and is about equal to 0.2. If $M = 10^5$ SWU/year (or, 100 tons of separation power per year), the average power required is $\overline{P}$ = 100 W. It may supply fuel to a 1 million kilowatt nuclear power plant.

If the overall efficiency of the laser system (electrical energy → copper laser → dye laser) is η_L = 0.1 percent, then the energy required in the separation of a ^{235}U atom is

$$E = \frac{h\nu(\sim 9\,eV)}{\eta_L \cdot \eta} = 30KeV$$

much less than the 3 MeV of the diffusion method.

V. Laser Atomic Uranium Separation Device

Figure 4 shows schematically the setup of the laser atomic uranium separation device. The system consists of two main parts: the laser system and the separation system. The laser system has three or four laser wavelengths and the last wavelength is used to excite the population of the energy state 620 cm^{-1} above the ground state. Each laser consists of a dye oscillator and an amplifier and all the dye lasers are pumped by the copper laser. Laser beams of different wavelengths must be accurately synchronized spatially and temporally in the separator. Only a few lasers are shown in the figure. In practice, for a medium plant of 10^6 SWU/year, the average power of the dye lasers is 10.000 W, the power of the copper vapor laser is several hundreds of thousand watts, and the total number of lasers may exceed 1000. The electrooptic industrial value of production associated with the laser atomic isotope separation is estimated to be several hundred million U.S. dollars per year.

The separator consists of an evaporator, an electromagnetic deflector, and a collector. The evaporator uses an electron gun and produces a 3500°K temperature on the uranium metal. The surrounding metal remains in the solid state, thus avoiding the corrosion of the crucible by the high temperature uranium metal. After selective ionization, the uranium vapor is deflected by the electromagnetic deflector and then collected. The tailing is collected directly in the tailing collector. Both collectors are operated at a temperature above the melting point of uranium so that the condensed liquid uranium is collected and the process proceeds continuously.

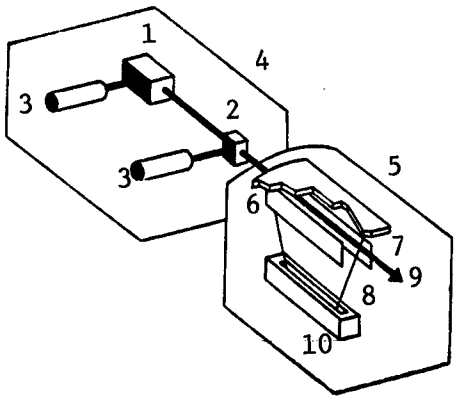

Key:
1. Main oscillator of dye laser
2. Amplifier of dye laser
3. Copper vapor laser
4. Laser system
5. Separator system
6. Product collector
7. Tailing collector
8. Steam
9. Laser beam
10. Vaporizer

Fig. 4. Schematic diagram for the atomic laser method of uranium isotope separation

VI. Physics and Engineering of the Process

The demonstration experiment of the laser atomic uranium isotope separation was completed in 1974. In order for the laser atomic method to replace the current diffusion method, a miriad of physics and engineering problems must be solved. Generally speaking, one needs to measure the spectral data of the uranium atom, select the optimum spectral line, understand the dynamics of the interaction between many strong lasers and a multienergy system, and investigate the properties of the high temperature uranium vapor. In terms of engineering, one needs to develop long life, high efficiency and low cost laser systems, high power electron guns and large volume, high vacuum systems, and understand how to process uranium compounds and the uranium metal.

REFERENCES

1. Lu Yingzhong, KEXUE [SCIENCE], Vol 8, 1982, p 1.

2. Laser Program Publication and Related Reports, LLL, 1976.

9698/7358
CSO: 4008/88

THEORY AND IMPLEMENTATION OF THE MULTIFUNCTIONAL LR PARSER GENERATION XYZ/PG

Beijing JISUANJI YANJIU YU FAZHAN [COMPUTER RESEARCH AND DEVELOPMENT] in Chinese Vol 23, No 6, 1986 pp 1-18

[English abstract of article by Dong Chun [5516 2504] of Institute of Software, Chinese Academy of Sciences]

[Text] A new approach for generating optimized and bypassed LR(K) parsers is proposed, and its correctness is proved. It can be used for obtaining parsers with much smaller size than that of the parsers generated by the well-known algorithm of Pager[11]. Furthermore, it has been programmed in PASCAL and implemented on NORD-500 computer system as well as DUAL MC 68000 system.)
(Paper received Sep 85.)

REFERENCES

[1] Aho, A. V & Ullman, J. D "Principle of Compiler Design", Addison-Wesley Publishing Company 1977.
[2] Aho, A. V & Ullman, J. D "Optimization of LR (k) Parsers", J. of Computer and System Science. 6, 573—602 (1972).
[3] Aho, A. V & Ullman, J. D "A Technique for Speeding up LR (k) Parsers", SIAM J. Comput. 2, 106—127 (1973).
[4] Anderson, T. & Eve, J. & Horning, J. J. "Efficient LR (1) Parsers", Acta Informat. 2, 12—39 (1973).
[5] 唐稚松: LR (k) 语法分解及 FPT 程序的优化,数学学报 21:1 (1978).
[6] 唐稚松: LBLR (k) 文法与文法分划,计算机学报 3:1 (1980).
[7] DeRemer, F. L. "Practical Translations for LR (k) Languages", Project MAC, Mass. Inst. of Tech., Cambridge, Tech. Report MAC TR-65, October 1969.
[8] DeRemer, F. L. "Simple LR (k) Grammars", Comm. ACM 14, 453—460 (1971).
[9] Knuth, D. E. "On the Translation of Languages from Left to Right", Information and Control 8 (1965), 607—639.
[10] Pager, D. "A Solution to an Open Problem by Knuth", Information and Control 17, 462—473 (1970).
[11] Pager, D. "A Practical General Method for Constructing LR (k) Parsers", Acta Informat. 7, 249—268 (1977).
[12] Pager, D. "Eliminating Unit Productions from LR Parsers", Acta Informat. 9, 31—59 (1977).
[13] Soisalon-Soininen, E. "On the Space Optimizing Effect of Eliminating Single Productions from LR Parsers", Acta Informat. 14, 157—174 (1980).
[14] Tokuda, T. "Eliminating Unit Reduction from LR (k) Parsers Using Minimum Contexts", Acta Informat. 15, 447—471 (1981).
[15] 冯玉琳: LBLR (k) 优化中的错误检测, «计算机学报»3:3 (1980).

A DESIGN METHOD FOR THE 68000C ANTI-COMPILER

Beijing JISUANJI YANJIU YU FAZHAN [COMPUTER RESEARCH AND DEVELOPMENT] in Chinese Vol 23, No 6, 1986 pp 32-36

[English abstract of article by Liu Zongtian [0491 1350 3944] of Hefei Industrial University]

[Text] The construction and a design method for the 68000C anti-compiler are presented. The anti-compiler consisting of three components, namely, lexical analyzer, symbolic list generator and statement translator, can translate a program in the 68000 assembler language into another program in the C language. The method of distinguishing symbolic attributes by some rules is used in the symbolic list generator and the technique of symbolic execution and program transformation is used in the statement translator.) (Paper received Sep 85.)

REFERENCES

[1] 周孔伟、蔡经球，符号执行——介于程序验证和程序调试之间的方法，小型微型计算机系统，1982年，第4期。

[2] 刘宗田，ADL语言及其在程序展开中的应用，计算机学报，1986年第1期。

COMPUTER-AIDED ANALYSIS SYSTEM FOR MEDICAL GRAPHS

Beijing JISUANJI YANJIU YU FAZHAN [COMPUTER RESEARCH AND DEVELOPMENT] in Chinese Vol 23, No 6, 1986 pp 53-57

[English abstract of article by Gong Liping [1362 0500 1627] of Beijing Medical College and Sun Kai [1327 0418] of Jiangxi Institute of Metallurgy]

[Text] A computer-aided analysis system in which technique of electromagnetic induction is used as a way of graphic input is described. It illustrates hardware and software designs, basic theory, function and structure of electromagnetic digitizer. Then it describes methods and procedures of graphing and monitoring as well as development of applied software. The system, employing electromagnetic pen or venier as a medium for transmitting data, easily fulfills the input of two-dimensional graphs by means of assembler. It provides a reliable and convenient facility in studying and analysing graphs.) (Paper received Aug 85.)

REFERENCES

[1] H. Haber-Schain, J. B. Cross, J. H. Dodge, J. A. Walter, "PSSC Physics", D. C. Health, 1971, 3rd ed.
[2] R. K. Brayton, "Optimization in Computer-aided Circuit Design", IBM Research Report RC 7159 (#30683), September 1978.
[3] ANDREWS, H. C., "Computer Techniques in Image Processing", Academic Press, New York and London, 1970; see also IEEE Transactions on Computers, C-20 No. 9, Sept. 1971, 1045—1051.
[4] F. Greenberger edited, "Computer Graphics Utility/Production/Art", Academic Press, 1967.
[5] Forrest, A. R., "Co-ordinates, Transformations, and Visualization Techniques", CAD Group Document No. 23, Cambridge University, June 1969.

/7358
CSO: 4009/1098

THE EFFICACY OF TAI-DING-AN ON THE INHIBITION OF HSV-I SKIN INFECTIONS IN GUINEA PIGS

Beijing YAOXUE XUEBAO [ACTA PHARMACEUTICA SINICA] in Chinese Vol 21, No 4, 29 Apr 86 pp 252-255

[English abstract of article by Chen Hongshan [7115 7703 3790], et al., of Institute of Antibiotics and Institute of Materia Medica, Chinese Academy of Medical Sciences, Beijing]

[Text] Tai-Ding-An (TDA) (3-phthalimido-2-oxo-butyraldebisthiosemicarbazone) is a derivative of thiosemicarbazone with anti-chlamydozoa trachomatis activity and was used in clinic for treatment of trachoma in China. Tai-Ding-An was found to have anti-herpetic activities both in cell cultures and in guinea pig skin infections. Tai-Ding-An is insoluble in water but soluble in DMSO. 1~2% TDA in 60% DMSO applied topically on HSV-I infected guinea pig skin, QID for 5 days, started 24 hrs after infection significantly inhibited the development of skin lesions. Since 2% TDA in 60% DMSO is a saturated solution, TDA precipitated on the skin and interfered with the healing of the lesions, so that it was less active than that of 1% TDA. 0.25% TDA in 25% DMSO and 2% TDA paste gave no significant therapeutic effect. (Paper received 24 Nov 84.)

REFERENCES

1. 赵知中等. 治疗沙眼新药——酞丁安的合成. 科学通报 1979; (3):142.
2. 赵知中等. "酞丁安"的合成研究. 化学学报 1980; 38:67.
3. 陈祖基等. 醛酮缩氨基硫脲类化合物抗沙眼衣原体的实验研究. 药学通报 1980; 15:482.
4. 朱钵等. 酞丁安治疗带状疱疹 78 例疗效观察. 中华医学杂志 1982; 4:212.
5. 袁兆庄等. 关于酞丁安治疗病毒性皮肤病的报告. 中华医学会全国皮肤科学术会议摘要 1982; 140.
6. 朱钵等. 酞丁安治疗尖锐湿疣 12 例报告. 临床皮肤科杂志 1982; (4):175.
7. 谢晶晖等. 酞丁安治疗病毒性皮肤病 140 例报告. 同上 1984; (4):47.
8. 尹明标等. 酞丁安对单纯疱疹病毒在细胞培养内复制的影响. 药学学报 1984; 19:387.

SELECTIVELY ANTIMETASTATIC EFFECTS OF ARYLTRIAZENE METHOXYPYRIMIDINE ON LEWIS LUNG CARCINOMA

Beijing YAOXUE XUEBAO [ACTA PHARMACEUTICA SINICA] in Chinese Vol 21, No 4, 29 Apr 86 pp 256-259

[English abstract of article by Jiang Chun [3068 2504] and Li Dehua [2621 1795 5478] of Tianjin Institute of Medical and Pharmaceutical Sciences, Tianjin]

[Text] ATMP, 4 [p-(3,3-dimethyl-1-triazene) phenylsulfamide]-5,6-dimethoxy-pyrimidine was first synthesized by Tianjin Institute of Medical and Pharmaceutical Sciences. Effects of ATMP have been studied in comparison with those of cyclophosphamide (CY) in mice bearing Lewis lung carcinoma. At the dosages of 10, 20, and 40 mg/kg/d, ATMP was shown to inhibit the number and the weight of spontaneous pulmonary metastasis but showed no significant effect on the primary tumor. Antimetastatic effects were also demonstrated by histological exmination. On the contrary, CY 18 mg/kg/d ip obviously inhibited the growth of both primary tumor and pulmonary metastasis, whereas under relatively lower dosage, no effects on the tumors of both locations were observed. The effects of the two agents on the fractional incorporation of ^{3}H-TdR in tumor cells further indicated that at the dosage used in the experiment only ATMP was devoid of cytotoxic action for the primary tumor. The experiments also showed that ATMP did not modify the activity of Fc receptor of peritoneal macrophage in mice and did not reduce artificial metastasis. In the host pretreated with ATMP, no reduction of the formation of spontaneous metastasis was found.

These data indicate that ATMP, differing from CY, has selective antimetastatic effects. It acts directly on tumor cells and presumably inhibits their release from primary tumor into the bloodstream. (Paper received 21 Jun 85.)

REFERENCES

1. Hellmann K and Burrage K. Control of malignant metastasis by ICRF-159. *Nature* 1969;224:237.
2. Heyes J. Antimetastatic effects of 4-carbethoxy-5-(3,3 dimethyl-1-triazene)-2-methylimidazole. *J Natl Cancer Inst* 1974;53:279.
3. 刘纪云等. 芳基三氮烯化合物的合成. 医药工业 1984;(9):20.
4. Giraldi T, et al. Antimetastatic action of some triazene derivatives against the Lewis lung carcinoma in mice. *Cancer Treat Rep* 1978;62:721.
5. 马克韶等.刺参酸性粘多糖抗肿瘤肺转移的实验研究.海洋药物 1982;(1):21.
6. Houghton PJ, et al. effects of cytotoxic agents on TdR incorporation and growth delay in human colonic tumor xenografts. *Br J Cancer* 1977;36:206.
7. 朱云风.小鼠腹腔巨噬细胞 Fc 受体的观察.上海免疫学杂志 1982;2:65.
8. Giraldi T, et al. Selectivity of the antimetastatic and cytotoxic effects of 1-p-(3,3 dimethyl triazene) benzoic and potassium salt (±)-1,2-di (3,5 dioxopiperazin-1-yl) propane and cyclophosphamide in mice bearing Lewis lung carcinoma. *Cancer Res* 1981;41:2524.
9. Ross E and Dingemans K. Mechanism of metastasis. *Biochim Biophys Acta* 1979;560:135.
10. Jams SE and Salsbury AJ. Effects of(±) 1,2 bis (3,5 dioxopiperazin-1-yl) propane on tumor blood vessels and its relationship to the anti metastatic effect in the Lewis lung carcinoma. *Cancer Res* 1974; 34:839.

CHROMATOGRAPHY OF BUNGARUS FASCIATUS VENOM AND PRELIMINARY STUDIES OF ITS NEUROTOXIN--FRACTION IX

Beijing YAOXUE XUEBAO [ACTA PHARMACEUTICA SINICA] in Chinese Vol 21, No 4, 29 Apr 86 pp 260-264

[English abstract of article by Kong Jianqing [1313 0256 1730] and Wu Xiurong [0702 4423 2837] of Department of Pharmacology, Zhongshan Medical University, Guangzhou]

[Text] A neurotoxin, Fraction IX, was separated from the venom of Bungarus fasciatus by CM-Sephadex C 50 chromatography. The fraction blocked both the neuromuscular transmission of chicken biventer cervicis muscle and the response of the preparation to acetylcholine with a long latent period (134±49 min). Whereas, the responsibilities of the muscle to direct stimulation or high concentration of potassium chloride were not affected; not many contractures were found in the preparation. In frog sartorius muscle, fraction IX inhibited the amplitudes of endplate potential (EPPs) and miniature endplate potentials (mEPPs). Neither the frequencies of miniature endplate potential nor the resting membrane potential of the muscle were changed by fraction IX. According to the experiments, it was suggested that fraction IX is a postsynaptic neurotoxin. (Paper received 25 Jul 85.)

REFERENCES

1. Bon C and Changeux JP. Chemical and pharmacological characterization of toxic polypeptides from the venom of Bungarus caeruleus. *Eur J Biochem* 1977;74:31.
2. Bon C and Changeux JP. Ceruleotoxin: a possible marker of the cholinergic ionophore. *Ibid* 1977; 74: 43.
3. Lee CY. Recent advances in chemistry and pharmacology of snake toxins. In: Ceccarelli B. and Clementi F. ed 5 *Advance of Cytopharmacology* Vol 3. New York: Raven Press, 1979:1～16.
4. Raftery M. et al. Properties of Torpedo californica acetylcholine receptor *Ibid* 1979:159～182.
5. Bon C and Saliou B. Isolation of "ceruleotoxin" from *Bungarus fasciatus* venoms. *Toxicon* 1982; 20: 111.
6. 孔健强、吴秀荣.金环蛇(*Bungarus fasciatus*) 蛇毒的分离及其毒性组分的药理研究.药学学报 1983;18:97.
7. 四川医学院主编. 卫生统计学. 第1版. 北京: 人民卫生出版社,1978;91～93.
8. Ginsborg BL and Warriner J. The isolated chick biventer cervicis nerve-muscle preparation. *Brit J Pharmacol* 1960;15:410.
9. 陈式樱等.金环蛇 (*Bungarus fasciatus* Schneider) 蛇毒的研究 I. 金环蛇蛇毒毒性组分的分离纯化与鉴定.生物化学与生物物理学报 1981; 13:535.
10. Chang CC. The action of snake venom on nerve and muscle. In: CY LEE, ed. *Handbook of Experimental Pharmacology* Vol 52. Snake venoms. Berlin:Springer-Verlag, 1979:309～376.
11. 杨钦照、徐科. 蝮蛇毒的神经毒成分的研究. 生物化学与生物物理学报 1977;9:357.
12. Su C. et al. Pharmacological properties of neurotoxin of cobra venom. In: Russell FE and Saunders PR. eds. *Animal toxins*. Oxford: Pergamon Press, 1966:259～267.
13. 仇慧芳、吴秀荣. 眼镜王蛇 (*Ophiophagus hannah* Cantor)毒的分离及毒性组分的研究. 药学学报 1983;18:161.

SYNTHESIS OF ANTICHOLINERGIC COMPOUNDS α-CYCLOPENTYLPHENYLMETHOXY-ALKYLAMINES

Beijing YAOXUE XUEBAO [ACTA PHARMACEUTICA SINICA] in Chinese Vol 21, No 4, 29 Apr 86 pp 265-272

[English abstract of article by Gao Jianhua [7559 1696 5478], et al., of Institute of Pharmacology and Toxicology, Academy of Military Medical Sciences, Beijing]

[Text] A series of α-cyclopentylphenylmethoxyalkylamines were synthesized. Cyclopentyl phenyl ketone was obtained by Grignard reaction of bromocyclopentane and benzonitrile. When cyclopentyl phenyl ketone was reduced by lithium aluminum hydride it gave the pure alcohol correspondingly, and the yield was higher than that of any previous methods. Dehydration of α-cyclopentylphenylmethanol would take place in the presence of acid and a similar intra-molecular elimination of α-cyclopentyl-α-chloro-toluene would occur in the presence of base, both forming benzalcyclopentane. Compounds IV-1~IV-4 were obtained by 1 mole of α-cyclopentylphenylmethanol reacting with 1 mole of chloroaminoalkanes in the presence of 1.1 mole of sodium hydride, yields 40~80 percent; 1 mole of α-cyclopentyl-α-chloro-toluene reacted with 2 mole of alkamines to give compounds IV-5~IV-9 in yields of 17~37 percent. The hydrochlorides or oxalates and methyl iodides of the compounds exhibited anticholinergic activities in mice. (Paper received 3 Apr 85.)

REFERENCES

1. Feinberg SM. Histamine and antihistaminic agents——Their experimental and therapeutic status. *J Am Med Assoc* 1946;132:702.
2. Harms AF and Nauta WT. The effects of alkyl substitution in drugs. I. Substituted dimethylaminoethyl benzhydryl ethers. *J Med Pharm Chem* 1960;2:57.
3. Farquharson ME and Johnston RG. Antagonism of the effects of tremorine by tropine derivatives. *Brit J Pharmacol* 1959;14:559.
4. Ohnacker G and Kottler A. Ethers. *Ger Offen* 955595; *CA* 1959; 53:2166.
5. Rama Sastry BV. Anticholinergics: Antispasmodic and antiulcer drugs. In: Wolff ME. ed. Burger's Medicinal Chemistry. 4th ed. Part III. New York. Chichester. Brisbane.Toronto: John Wiley & Sons, 1973:390~391.
6. Nightingale DV and Maienthal M. The action of nitrous acid on 2-phenylcyclohexylamine. *J Am Chem Soc* 1950;72:4823.
7. Waugh TD and Boulder C. Production of carbinols employing cyclopentadienyl or lower alkyl substituted cyclopentadienyl Grignard reactions and hydrogenation. *US patent* 3381017; *CA* 1968; 69:26859.
8. Tilford CH and Van Campen MG. Diuretics. *a,a*-Disubstituted 2-piperidine-ethanols and 3,3-disubstituted octahydropyrid [1,2-c] oxazines. *J Am Chem Soc* 1954;76:2431.
9. Steven AR and Closson WD. The cyclopentylphenylcarbinyl cation system. *J Am Chem Soc* 1969; 91: 1701.

CONSTRUCTION AND ANALYTICAL APPLICATIONS OF ALL-SOLID-STATE CARBETAPENTANE ION-SELECTIVE ELECTRODE

Beijing YAOXUE XUEBAO [ACTA PHARMACEUTICA SINICA] in Chinese Vol 21, No 4, 29 Apr 86 pp 285-290

[English abstract of article by Yao Shouzhuo [1202 1343 2154], et al., of Institute of New Material Research, Hunan University, Changsha]

[Text] The construction and performance characteristics of all-solid-state carbetapentane ion-selective electrode are described. The electrode, based on ion-pair complex with phosphotungstate, showed rapid and Nernstian response to carbetapentane in the 1×10^{-7}~2×10^{-6}M concentration range with a cationic slope of 59 mV/logC. The electrode responses were not affected by pH in the range 2.2~7. Direct potentiometry and potentiometric titration in micro-volume were used to determine carbetapentane in pharmaceutical preparations, urine and blood with satisfactory results. (Paper received 8 Jun 85.)

REFERENCES

1. 姚守拙、程梅华.全固态链霉素传感电极的研制. 药学学报 1985; 20:450.
2. 中华人民共和国药典. 1977 年版.二部. 1978:344.
3. 姚守拙等. 维生素 B_1 选择性电极的研究. 药学学报 1983; 18:612.

SYNTHESIS OF 11-KETO-Δ^9-NORETHISTERONE

Beijing YAOXUE XUEBAO [ACTA PHARMACEUTICA SINICA] in Chinese Vol 21, No 4, 29 Apr 86 pp 300-302

[English abstract of article by Chen Wei [7115 3555] and Zhang Xingyue* [1728 2502 1471] of Synthesis Department of Shanghai Institute of Planned Parenthood Research, Shanghai; *Chemistry Department of Jiao Tong University, Shanghai]

[Text] We have introduced a carbonyl group at the 11-position and a double bond at the 9-position of norethisterone in order to increase its antifertility potency. The starting material for the preparation of 11-keto-Δ^9-norethisterone (9) was 19-hydroxy-Δ^4-androstene-3,17-dione(1), which was converted to the title compound by partial synthesis through the sequence of reactions: (1)→(9).

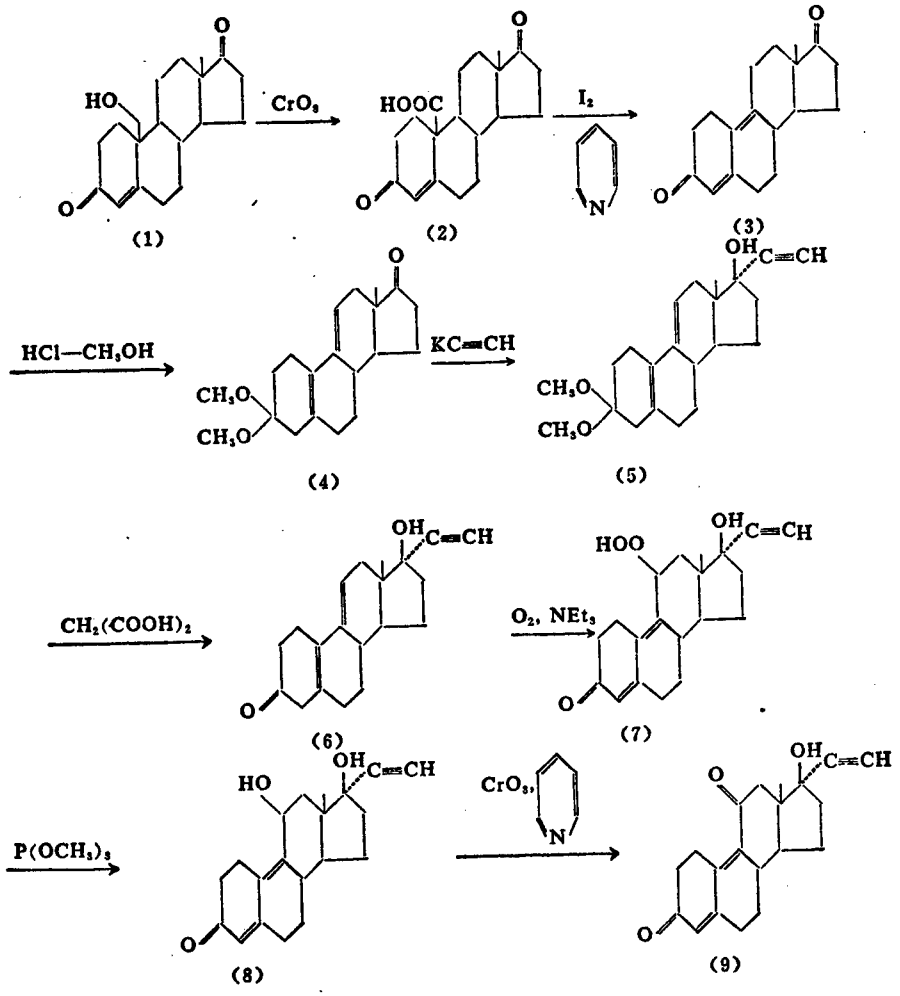

11-Keto-Δ^9-norethisterone was found to possess very potent antifertility effect by preliminary screening tests. (Paper received in 1985.)

REFERENCES

1. Mathieu J. *Proceedings of the International Symposium on Drug Research*. Montreal, 1967;134～158.
2. Roussel-Uclaf. Total synthesis of 13-alkyl steroids. *Neth Appl* 6,414,702;*CA* 1965;63.18222g.
3. Roussel-Uclaf. $\Delta^{4,9}$-3-Oxo-11 β-hydroxy-19-norsteroids. *Ger Offen* 1,229,526;*CA* 1967;68:55647j.
4. 中国科学院上海有机化学研究所甾族激素组，上海第九制药厂：口服避孕药三烯炔诺酮和 dl-18-甲基三烯炔诺酮的合成．化学学报 1975;33:139.

/7358
CSO: 4009/1091

STUDIES ON NONSTEROIDAL ANTIINFLAMMATORY DRUGS: SYNTHESIS AND BIOLOGICAL ACTIVITY OF 4-HYDROXY-3-AMINOMETHYL-DIPHENYL AND 4(2)-CYCLOHEXYL-2(4)-AMINO-METHYL-PHENOL DERIVATIVES

Beijing YAOXUE XUEBAO [ACTA PHARMACEUTICA SINICA] in Chinese Vol 21, No 5, 29 May 86 pp 345-355

[English abstract of article by Zhang Yinsheng* [1728 1377 3932], et al., of Nanjing College of Pharmacy, Nanjing]

[Text] With an attempt to search for potent nonsteroidal antiinflammatory drugs with less side-effects, twenty six derivatives of 4-hydroxyl-3-amino-methyldiphenyl and 4(2)-cyclohexyl-2(4)-aminomethylphenol were prepared by Mannich reaction. Nineteen of the compounds were tested in rats. Some of these compounds showed significant antiinflammatory and antipyretic-analgesic activities. Antiimplantation test was also carried out on twenty of the compounds, but none was found active.

REFERENCES

1. Sankawa U, et al. Depside as potent inhibitor of prostaglandin biosynthesis. *Prostaglandins* 1982; 24:21.
2. Schlege DC et al. Bulky amine analogues of ketoprofen: potent antiinflammatory agents. *J Med Chem* 1984; 27:1682.
3. Dewhirst FE, et al. Structure-activity relationship for inhibition of prostaglandin cyclooxygenase by phenolic compounds. *Prostaglandins* 1980; 20:209.
4. Moor GGI, et al. Antiinflammatory agents. *US Patent* 4,172,151; *CA* 1979; 90:103639 c.
5. Gomberg M, et al. Methylbiphenyl. *J Am Chem Soc* 1926; 48:1372.
6. Bruson HA, et al. Condensation of phenols with amines and formaldehyde. *Ibid* 1941; 63:270.
7. Grillot GF, et al. The condensation of diethylamine and formaldehyde with phenol, o-, m- and p-cresols. *Ibid* 1945; 67:1968.
8. Bruson HA, et al. Preparation of 2, 4, 6-tri-(dimethyl-aminomethyl)-phenol. *Org Reactions* 1942;1:330.
9. Bartlett JF, et al. Some cyclohexyphenols and phenol ethers *Zh Organ Khim* 1965;1:517; *J Am Chem Soc* 1927;49:2098.
10. Abdurasuleva AR, et al. Alkylation of cresols with cyclohexanol and cyclopentanol. *CA* 1965; 63:1722a.
11. Raiford LC, et al. 3-Nitro-4-hydroxydiphenyl and some of its derivatives. *J Am Chem Soc* 1925;47:1454.
12. Moir J, et al. New derivatives of diphenol. *J Chem Soc* 91:1305; *CA* 1908; 2:85.
13. Mueller GP. et al. Cis-and trans-1, 4-bis-(p-methoxyphenyl)-cyclohexane. *J Am Chem Soc* 1952; 74: 5631.

DEVELOPMENT AND PHARMACOKINETIC STUDY OF SUSTAINED RELEASE DOXYCYCLINE HYDROCHLORIDE PELLETS

Beijing YAOXUE XUEBAO [ACTA PHARMACEUTICA SINICA] in Chinese Vol 21, No 5, 29 May 86 pp 370-376

[English abstract of article by Qiu Yihong* [6726 1837 5725], et al., of Department of Pharmaceutics, Nanjing College of Pharmacy, Nanjing]

[Text] Encapsulated sustained-release doxycycline hydrochloride pellets (SRDP) were developed. SRDP was designed so that drug release was through a diffusion rate controlling membrane constituting the pellet coat and thus could be used to reduce the gastrointestinal injuries in human induced by doxycycline (DX). SRDP showed drug liberation pattern which was best described by zero-order kinetic equation with release constant being 20.5 mg/h; A tentative two-year expiration date on SRDP was established; The new dosage form was shown to be significantly less irritative to gastric mucosa than a commercially available conventional table (CCT,) ($p<0.001$), and no more irritating than a placebo. The blood concentration-time course was demonstrated to fit a classical one-compartment model with apparent zero order absorption and first order elimination. The parameters were calculated based on the individual and average serum level data using a NONLIN computer program with mean values of K_a, k, Vd, t_{max}, c_{max} being 58.08 mg/h, 0.032 h^{-1}, 82.21 L, 3.94 h and 2.30μg/ml, respectively. Information derived from observed data in vivo and the pharmacokinetic analysis suggested that during the usual therapeutic dosage regimens of DX, SRDH was bioequivalent to CCT. Moreover, in vivo drug availability well correlated with in vitro values. (Paper received 8 Jul 85.)

REFERENCES

1. 陈新谦. 新编药物学. 第11版. 北京: 人民卫生出版社, 1982:70.
2. Reynolds JEF. *Martindale the Extra Pharmacopoeia*. 28th ed. London: The Pharamaceutical Press, 1982:1155.
3. Rao GR, et al. Colorimetric determination of doxycycline hydrochloride. *East Pharm* 1981; 24:121.
4. Van den Bogert C and Kroon AM. Fluorometric determination of tetracyclines in small blood and tissue samples. *J Pharm Sci* 1981; 70:186.
5. Steinbuch Z and Möller H. Investigations into the accuracy of dosage and release of active drug from sustained release preparations of isosorbide dinitrate. *Int J Pharm* 1978; 1:197.
6. Faldmann SS. Consistency in stability testing. *J Pharm Sci* 1979; 68:1.
7. Yamaoka K, et al. Application of Akaike's information criterion (AIC) in the evaluation of linear pharmacokinetic equations. *J Pharmacokin Biopharm* 1978;6:165.
8. Gibaldi M and Perrier D. *Pharmacokinetics*. 2nd ed. New York: Marcel Dekker, 1982:149~153.
9. Vallner JJ, et al. A proposed general protocol for testing bioequivalence of controlled-release drug products. *Int J Pharm* 1983; 16:47.
10. Langenbucher F. Numerical convolution/deconvolution as a tool for correlating *in vitro* with *in vivo* drug availability. *Pharm Ind* 1982; 44:1166.

/7358
CSO: 4009/1092

- END -